Hindawi

Research Article

Stochastic Optimal Selection and Analysis of Allowable Photovoltaic Penetration Level for Grid-Connected Systems Using a Hybrid NSGAII-MOPSO and Monte Carlo Method

Ali Abubakar [ID],[1,2] **Reindorf Nartey Borkor** [ID],[1,2] **and Peter Amoako-Yirenkyi** [ID][1,2]

[1]*Department of Mathematics, Kwame Nkrumah University of Science and Technology, Kumasi, Ghana*
[2]*Center for Scientific Computing and Industrial Modelling, National Institute for Mathematical Sciences, Ghana*

Correspondence should be addressed to Ali Abubakar; aabubakar10@st.knust.edu.gh
and Peter Amoako-Yirenkyi; amoakoyirenkyi@knust.edu.gh

Generally, the main focus of the grid-linked photovoltaic systems is to scale up the photovoltaic penetration level to ensure full electricity consumption coverage. However, due to the stochasticity and nondispatchable nature of its generation, significant adverse impacts such as power overloading, voltage, harmonics, current, and frequency instabilities on the utility grid arise. These impacts vary in severity as a function of the degree of penetration level of the photovoltaic system. Thus, the design problem involves optimizing the two conflicting objectives in the presence of uncertainty without violating the grid's operational limitations. Nevertheless, existing studies avoid the technical impact and scalarize the conflicting stochastic objectives into a single stochastic objective to lessen the degree of complexity of the problem. This study proposes a stochastic multiobjective methodology to decide on the optimum allowable photovoltaic penetration level for an electricity grid system at an optimum cost without violating the system's operational constraints. Five cutting-edge multiobjective optimization algorithms were implemented and compared using hypervolume metric, execution time, and nonparametric statistical analysis to obtain a quality solution. The results indicated that a Hybrid NSGAII-MOPSO had better convergence, diversity, and execution time capacity to handle the complex problem. The analysis of the obtained optimal solution shows that a practical design methodology could accurately decide the maximum allowable photovoltaic penetration level to match up the energy demand of any grid-linked system at a minimum cost without collapsing the grid's operational limitations even under fluctuating weather conditions. Comparatively, the stochastic approach enables the development of a more sustainable and affordable grid-connected system.

1. Introduction

One of the key drivers of every country's economy is sustainable energy. The existing conventional energy sources (CES) such as coal, gas, and other oil-fired resources constitute a significant share (80%) of the global energy supply [1]. However, their environmental and economic effects have delimited their usage. The CES are predominant sources of pollution, rapid climatic changes, and global warming emissions [2]. Also, they are hardly sustainable and cost-effective.

They fluctuate rapidly with the potential to destabilize economies. The global energy demand currently exceeds the supply, causing an unpredictable power distribution and forcing rationing of power in many countries [3]. According to many studies, including [4], these effects can be reduced significantly by using renewable energy sources (RES). RES are environment-friendly and generate an insignificant amount of exhaust and other harmful gases [4]. RES are crucial power sources due to their sustainability. The desire to curb rapid emissions and lessen

dependency on foreign energy supplies has motivated many nations to make impressive strides in their energy systems by building larger RES systems.

The proportion of RES needs to be ramped up in order to keep up with future energy demand because it is anticipated that CES will lose some of its dominance in the near future [5].

In many applications, Solar Photovoltaic (SPV) resources seem substantially more sustainable, affordable, and reliable and contribute significantly to the electricity mix system than other RES [6]. Thus, this paper will focus on SPV due to its many applications.

The most challenging attributes associated with harnessing energy from the RES are their intermittency, availability, and the grid's technical limitations [7]. For instance, the production of SPV power is limited to the daytime. These challenges have technical solutions that foist unwelcome costs, which, if assigned to each RES project, will immensely affect their cost-competitiveness against conventional generation [7]. Another major hurdle to the large deployment of the SPV system globally is its relatively high cost. SPV system net costs are not constant and are greatly influenced by location-specific conditions such as resource quality and transmission mode.

In general, introducing SPV in our electricity grid has the potential of providing a substantial increase in total capacity [8–10]. But unless it is optimized, this might seriously create technical issues such as transmission and distribution losses, excessive reverse power flow, difficulty of islanding detection, harmonics, and degradation of voltage and frequency quality especially at a high penetration level of SPV electricity due to the intermittency and the fluctuations in the SPV output [11]. When there is any voltage or frequency fluctuation, the inverter disconnects the SPV system from the grid, and this leads to SPV power losses.

Therefore, a special design with a stronger focus on achieving a trade-off between minimum overall SPV system cost and high system reliability is mandatory [12]. A Hybrid Energy Supply System (HESS) formed by integrating multiple energy sources could give a much more reliable and cost-effective energy supply system [3, 13]. HESS is a gateway to deploying more affordable RES technologies that would eventually replace the CES [14]. The HESS has many design applications. This study focuses on the grid-connected system, which entails a connection to the power grid to either export the RES's ample energy production or purchase power during blackouts. This architecture might help lessen the heavy reliance on the CES.

Generally, the main focus of the grid-linked SPV systems is to scale up the SPV penetration level to ensure full electricity consumption coverage. However, due to the stochastic and nondispatchable nature of SPV generation, significant adverse impacts such as power overloading, voltage, harmonics, current, and frequency instabilities on the utility grid arise [15]. These impacts vary in severity as a function of the degree of penetration level of the SPV system [16].

Various authors are continuously investigating and reporting on this. Many have argued that the quick implementation of this smart technique would impose enough stress on many national grids. For instance, [15] stated that feeding the existing grid with a high SPV penetration level could degrade the smooth operations of the grid's characteristics. Reference [16] reported that if the grid's system was not technically structured, integrating a larger SPV system would cause significant power distortions. A critical and comprehensive review by [17] revealed that the surplus SPV power adversely affects the entire grid system during peak-power generation. Also, scaling up SPV penetration linearly affects the cost of the HESS design due to the high cost of SPV modules, inverters, and cables [18]. Reference [19] stated that it is no exaggeration to say that power supply systems under current circumstances are not yet ready to accommodate the expected increase in SPV penetration.

To deal with this problem, strategies like upgrading the power infrastructure (technological improvement) might address most of these issues, but it is not economically desired due to the incurred high-capacity costs [16, 20, 21]. Also, the Power Limiting Control (PLC) strategy proposed by [22] where the maximum SPV output power is constrained to some level especially during the midday in the Harmattan season is also a suitable option, but this could result in a significant SPV power loss [18, 23, 24]. Again, setting up excess storage systems could help increase and regulate the grid SPV penetration level [25] and enhance the entire system flexibility, but this solution is also not cost-viable to date [13, 14, 18, 26]. This calls for critical scientific techniques based on optimization, modelling, and control [27]. Also, one of the challenges in scaling up the SPV penetration in general is a function of their costs compared to conventional generation [28]. This is due to the high cost of the modules, inverter, cables, and other components in the SPV power generation system. The need for optimal design has inspired many authors. For instance, using the Transient Energy System Simulation Program software (TRNSYS), [29] built a deterministic sizing technique for a household HESS. The Strength Pareto Evolutionary Algorithm (SPEA) was used by [30] to schedule the best possible economic activities for grid-connected systems. A hybrid SPV/wind/battery energy storage system was sized using the Nondominated Sorting Genetic Algorithm II (NSGA-II) and Multiobjective Particle Swarm Optimization (MOPSO) methods by [2]. Reference [31] studied the impact of high penetrations on the harmonic level and proposed a simple and low-cost solution to dynamically vary the settings of the inverter's filter elements against irradiance. NSGA-II was used to build a grid connection that consists of a solar SPV and battery storage system in [32]. Reference [33] used a metaheuristic approach to design a HESS and concluded that considering the equipment's production rate would provide designers of such systems with a more accurate and realistic perspective. The fuzzy PSO was also used by [34] to size a HESS optimally, and the outcome showed that the method could produce quality solutions. Reference [35] constructed a HESS using artificial intelligence. In [36], an optimal harmonic reduction technique was performed to analyze and address harmonic distortions on large HESS distribution networks in Saudi

Arabia. Reference [37] used a PVsyst and ETAP to ensure optimal penetration of large-scaled HESS. An optimal planning solar SPV HESS consisting of solar SPV and battery storage systems for a HESS residential sector was designed in [17]. The study [8] built an optimization tool for SPV HESS using a nonlinear back-stepping controller. Reference [38] developed an advanced metering infrastructure and energy storage to reduce technical disturbances as a result of high penetration of RES. Another recent study by [39] performed a detailed power quality assessment of Karabuk University's grid-connected microgrid under high penetration of SPV generation and proposed optimal strategies to mitigate its effect on the grid. The studies [17, 40–45] provided detailed insight of the current development of optimization and control strategies for grid-connected systems.

The novel scientific findings in this study are summarized as follows. Though many existing design methodologies have tackled the problem in different forms, the effect of the variations in the problem is mostly ignored [5]. Few works that captured this effect mostly focused on scalarizing the stochastic multiple-objective problem into a stochastic single-objective problem to lessen the degree of complexity of the problem, although the design problem involves concurrently optimizing the multiple objectives in the presence of uncertainty [42]. On a critical review, studies like [46, 47] considered both the problem's stochasticity and the conflicting nature. However, they assumed there were no technical challenges to the SPV integration on the grid. This is critical as [19, 48] stated that it is not realistic enough to assess the system level of reliability if the technical impacts are ignored. According to [5], technical impacts on the HESS caused by large SPV penetration with minimal system cost have not been carried out broadly to date. This study captures the randomness and maintains the conflicting nature of the objectives. Again, the design problem propagates through all stages in the HESS design process. Unfortunately, existing methodologies target the design problem at individual parts of the HESS. In other words, they tackled the problem either at the generation (optimize production), transmission (sizing inverters), or distribution stage (dealing with technical connection challenges) [19]. Thus, a robust and complete optimal design strategy that addresses the problem at all stages does not exist [44]. This design approach holistically selects key variables required to optimize both cost and penetration level at each part of the HESS. Also, to optimize the SPV penetration level, one primary concern is the shading effect. One of the robust shading control mechanisms is the optimal regulation of the SPV system field parameters [49]. Authors in [50] considered this strategy; nevertheless, they failed to address the uncertainties in the design problem. Lastly, this study comprehensively examines and compares the state-of-the-art Multiobjective Evolutionary Algorithms using standard hypervolume metrics and consequently marks the Hybrid NSGAII-MOPSO to handle the design problem.

Therefore, to the extent of our knowledge, there is no existing complete design approach that preserves the multiobjective (optimizing SPV penetration level and cost)

nature of the design problem and stochastically represents the uncertainty concurrently without violating the grid's operational constraints at all stages in the HESS design process.

Thus, the main objective of the study is to build a stochastic multiobjective methodology for deciding the optimum maximum allowable penetration limit for SPV electricity at a minimum cost without violating a system's operational constraints. In addition, the modelling strategy addresses the shading effect by optimizing SPV field parameters. It would assist engineers in measuring the highest SPV power that a grid system could accommodate without violating its operational constraints, even under variable and nondispatchable RES.

The study is divided into the following sections: background, major findings, theoretical and methodological contributions to the design challenge, problem description, and objectives are all summarized in the first section. Section 2 also covers the objective function, constraints, and general design methodology. The design technique is validated in Section 3, and the simulation results are discussed. Section 4 consists of the conclusion and future recommendations.

2. Methodology

This paper seeks to optimize two conflicting objectives: net present cost ($C_{\text{net}}(\$)$) and maximum allowable SPV penetration level ($P_L(\%)$). Detailed mathematical modelling of the HESS is carried out to obtain these objective functions with all the grid operational constraints. Finally, the multiobjective optimization algorithm (MOOA) suitable for solving these conflicting objectives coupled with the Monte Carlo Approximation (MCA) is also discussed.

2.1. Estimation of the Net Present Cost. The total current cost of the HESS is calculated by deducting the sum of all current income from costs over its whole life. The following assumptions are considered: the system's lifetime is assumed to be 25 years, and any excess power generated by the SPV panel is transferred to the electricity system to make a profit. The economic model captures both discount and inflation rates, and only the inverter and wires will need to be changed over time.

The net present cost is estimated as follows:
Initial cost:

$$C_{\text{in}} = \left(N_p + N_s\right)C_{\text{spv}} + I_c C_{\text{inv}} + A_w C_w + C_I, \qquad (1)$$

where C_{spv}, C_{inv}, and C_w are the SPV, inverter, and cable unit costs, respectively, and N_p, N_s, I_c, and A_w represent parallel-connected panels, series-connected panels, and capacities of the inverter and cable, respectively.

When there is an inadequate SPV power supply, the traditional grid power would be a backup. Its cost is given as

$$C_g = G_g P_g F(r, f, T). \qquad (2)$$

G_g and P_g are the grid's electricity tariff and power, respectively. The series present worth factor, $F(r, f, T)$, is given as [51]

$$F(r, f, T) = \left(\frac{1+f}{r-f}\right)\left[\frac{1 - ((1+f)/(1+r))^T}{(1+r)^T}\right]. \quad (3)$$

Replacement and maintenance cost (C_m) is given as [46]

$$C_m = \left[(N_p + N_s)M_{spv} + I_c M_{inv}\right] F(r, f, T)(I_c R_{inv} + A_w R_w)K(r, f, J), \quad (4)$$

where M_{spv} and M_{inv} are the SPV and inverter unit maintenance costs, respectively; R_{inv} and R_w are the inverter and cable unit replacement costs, respectively; and J is the component's lifetime.

The $K(r, f, J)$ represents the single payment present worth factor stated as [47]

$$K(r, f, J) = \sum_{n=1}^{Y}\left[\left(\frac{1+f}{1+r}\right)^{J \times n}\right]. \quad (5)$$

Y represents the number of inverters and cables to be replaced.

The system's income: we assume that salvage value accrues at the end of the project lifetime. The present value of the system's salvage value of the inverter and the cable is given as [46]

$$S_I = C_{r_{inv}}(1 - D_{inv})^{L_{inv}} + C_{r_w}(1 - D_w)^{L_{iw}}. \quad (6)$$

$C_{r_{inv}}$ and C_{r_w} are the inverter and cable's replacement cost, respectively; L_{inv} and L_{iw} are the inverter and cable's lifetime, respectively; and D_{inv} and D_w are the depreciation rates of the inverter and cable, respectively.

The present value of the grid sale is given as [51]

$$G_I = K_{spv} \times P_{pv} \times F(r, f, T), \quad (7)$$

where P_{pv} is the SPV total generated power and K_{spv} is the SPV feed-in tariff. Considering all the costs and the income, the C_{net} can be calculated as

$$C_{net} = (C_{in} + C_m + C_g) - (S_I + G_I). \quad (8)$$

From Equations (1), (4), (2), (6), and (7), Equation (8) becomes
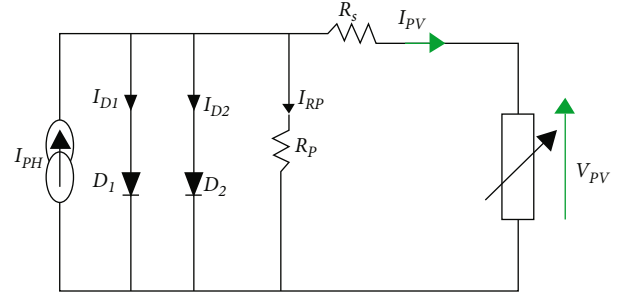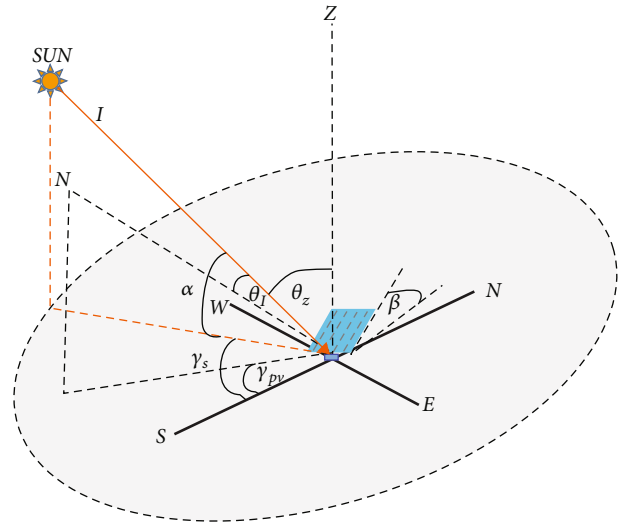

FIGURE 1: SPV cell equivalent circuit.

FIGURE 2: The geometry of the SPV system.

$$
\begin{aligned}
C_{net} = \Bigg\{ & (N_p + N_s)C_{spv} + I_c C_{inv} + A_w C_w + C_I \\
& + \left((N_p + N_s)M_{spv} + I_c M_{inv}\right) \\
& \cdot \left(\frac{1+f}{r-f}\right)\left[\frac{1 - ((1+f)/(1+r))^T}{(1+r)^T}\right] \\
& + (I_c R_{inv} + A_w R_w)\sum_{n=1}^{Y}\left[\left(\frac{1+f}{1+r}\right)^{J \times n}\right] \\
& + G_g P_g\left(\frac{1+f}{r-f}\right)\left[\frac{1 - ((1+f)/(1+r))^T}{(1+r)^T}\right]\Bigg\} \\
& - \Bigg\{ C_{r_{inv}}(1 - D_{inv})^{L_{inv}} + C_{r_w}(1 - D_w)^{L_{iw}} \\
& + K_{spv}[(P_{inv} - P_d) > 0]\left(\frac{1+f}{r-f}\right) \\
& \cdot \left[\frac{1 - ((1+f)/(1+r))^T}{(1+r)^T}\right]\Bigg\}.
\end{aligned}
\quad (9)
$$

2.2. Modeling of the SPV Penetration Level (P_L).

The SPV penetration level, defined as the percentage of electrical power provided by the RES [31], is introduced to assess the maximum

TABLE 1: Specifications of the SPV (monocrystalline) system.

Parameter	Value	Source
Grid's frequency range (Hz)	49-51	[62]
Grid's voltage range (V)	211-264	[62]
Total power capacity (kW)	10	[63]
Peak power (kW)	320	[63]
Efficiency	19.60	[52]
Rated voltage (V)	54.70	[63]
Rated current (A)	5.86	[63]
Open circuit voltage (V)	64.80	[63]
Short circuit current (A)	6.24	[63]
Efficiency of cables	93%	[52]
Efficiency of inverter	98.2%	[52]
Inverter's capacity (kW) range	1.5-10	[64]
Temperature coefficients (%/K)	-0.38	[63]
NOCT (°C)	45 ± 2	[63]
SPV cable range (mm^2)	(1.5-240)	[65]
Inverter voltage range (V)	200-400	[66]
Inverter current range (A)	7.5-25	[67]
Cable current-carrying capacity (amps)	775	[65]

SPV capacity that the distribution network can accommodate. By the IEEE standard 519-2014, there exists a series of operational restrictions on the maximum P_L in the grid system. The SPV penetration level is given by [4, 31, 52, 53]

$$P_L(t) = \frac{P_{pv}(t)}{\sum_{i=1}^{m} P_i(t)} \times 100\%, \tag{10}$$

where $P_{pv}(t)$ is the SPV power output defined as [52]

$$P_{pv}(t) = V_{pv}(t) \times I_{pv}(t) \cos(\theta) I_c \times A_w \times \eta_r \times \eta_v \\ \times \eta_l \times \eta_p \times [1 - \alpha_s(T_c - T_f)]. \tag{11}$$

The total power in the HESS given as

$$\sum_{i=1}^{m} P_i(t) = P_{pv}(t) + P_g(t). \tag{12}$$

$P_g(t)$ is the backup power from the grid, θ denotes the power factor, η_p is the power conditioning efficiency, η_r is the SPV reference efficiency, η_l is the efficiency because of losses in power in the cables (≈ 0.98), η_v is due to losses in the inverter (≈ 0.95), α_s is the temperature coefficient, T_c is the cell temperature, T_f is the SPV reference temperature, $I_T(t)$ is the global solar irradiance, T_a is the ambient temperature, A_u is the surface of the system unit, and T_N is the nominal operating cell temperature. The $V_{pv}(t)$ and $I_{pv}(t)$ are the SPV cell voltage and currents obtained by modeling a two-diode SPV cell, respectively, as shown in Figure 1.

The detailed modelling of the SPV current and voltage could be found in [49, 54–57], and they are as follows:

$$I_{pv}(t) = [I_{sc} + T_i(T_c - T_f)] \\ \cdot \frac{I_T}{1000} \left\{ \frac{I_{sc} + T_i(T_c - T_f)}{\exp[(V_{oc} + T_v(T_c - T_f))/V_t] - 1} \right\} \\ \cdot \left\{ \left[\exp\left(\frac{V_{pv} + I_{pv}R_s}{n_1 V_{t1}} \right) - 1 \right] - \left[\exp\left(\frac{V_{pv} + I_{pv}R_s}{n_2 V_{t2}} \right) - 1 \right] \right\} \\ - \frac{V_{pv} + I_{pv}R_s}{R_p}, \tag{13}$$

where T_c is given by [56, 57]

$$T_c = T_a + \left(\frac{T_N - 20}{80} \right) I_T. \tag{14}$$

To estimate irradiance, the anisotropic model of Klucher developed from the Coulson and Temps and Liu and Jordan models for every condition of the sky, like almost clear, clear, and cloudy, was employed. The details of the model can be found in the references [3, 50, 57–59], and it is defined as

$$I_T = \left(\frac{\cos \theta_i}{\cos \theta_z} \right) I_b + \left\{ \left[\frac{1}{2} \left(1 + \cos\left(\frac{\beta}{2} \right) \right) \right] \\ \cdot \left[1 + \left(1 - \left(\sqrt{\frac{I_d}{I_H}} \right)^2 \right) \cos^2 \theta_i (\sin^3 \theta_z) \right] \\ \cdot \left[1 + \left(1 - \left(\sqrt{\frac{I_d}{I_H}} \right)^2 \right) \sin^3\left(\frac{\beta}{2} \right) \right] \right\} \\ \cdot I_d + \left(\frac{1 - \cos \beta}{2} \right) \rho I_H + (K - 1) \\ \cdot \left\{ R_b I_b \left\{ 1 - \left[1 - \left(\frac{d \sin(\beta) + \cos(\beta)}{\cos(\beta) + [\sin(\beta)\cos(\gamma_s - \gamma_{spv})/\tan(\alpha)]} \right) \right] \right. \right. \\ \left. \cdot \left[1 - \left(\frac{d \sin(\beta) + \cos(\beta)}{l} \right) \left(\frac{|\sin(\gamma_s - \gamma_{spv})|}{\cos(\beta)\sin(\alpha) + \sin(\beta)\cos(\beta)} \right) \right] \right\} \\ + R_d I_d \left[\frac{\cos(1 + \beta)}{2} - \frac{1}{2} \left(\sqrt{d^2 + 1} - d \right) \right] \\ + \rho H \frac{1}{2} \left[\frac{D}{H} + 1 - \sqrt{ \left(\frac{D}{H} \right)^2 + \frac{2D}{H} \cos(\beta) + 1 } \right] \right\}, \tag{15}$$

where

$$\cos \theta_i = \sin \delta \sin \phi \cos \beta - \sin \delta \cos \phi \sin \beta \cos(\gamma_s - \gamma_{SPV}) \\ + \cos \delta \cos \phi \cos \beta \cos \psi \\ + \cos \delta \sin \phi \sin \beta \cos(\gamma_s - \gamma_{SPV}) \cos \psi \\ + \cos \delta \sin \beta \sin(\gamma_s - \gamma_{SPV}) \sin \psi$$

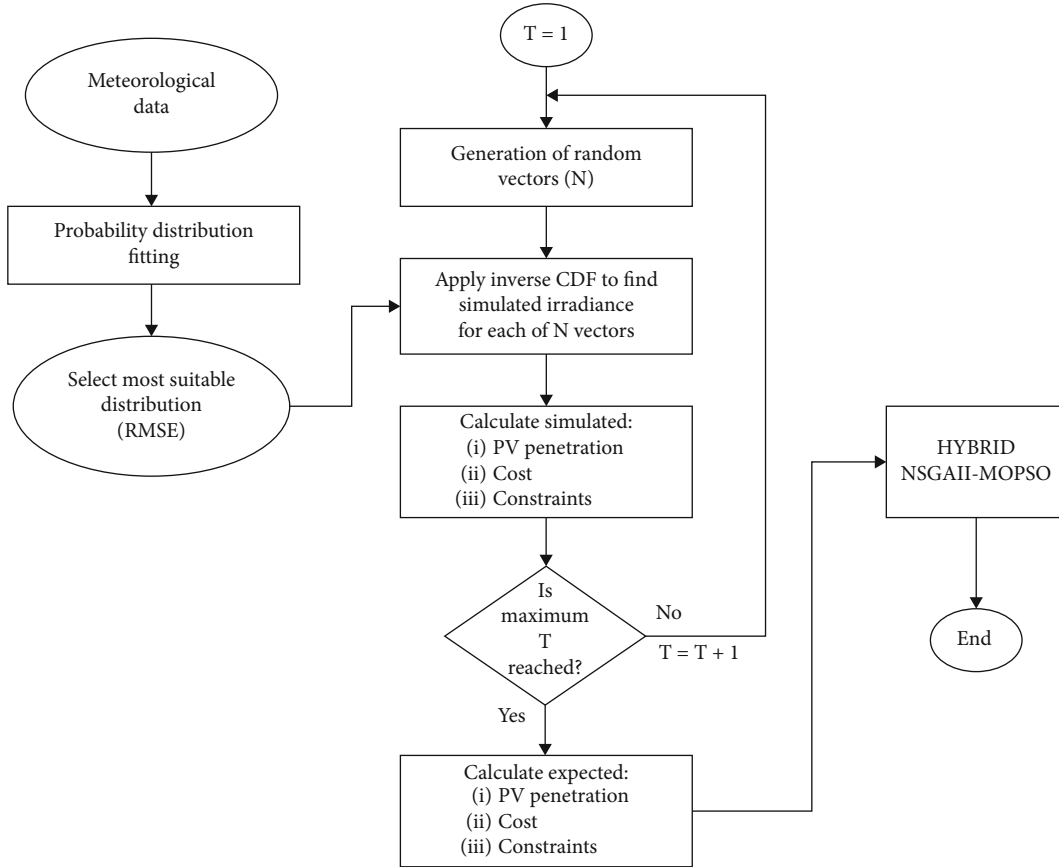$$\cos \theta_z = \cos \delta \cos \psi \cos \phi + \sin \delta \sin \phi. \tag{16}$$

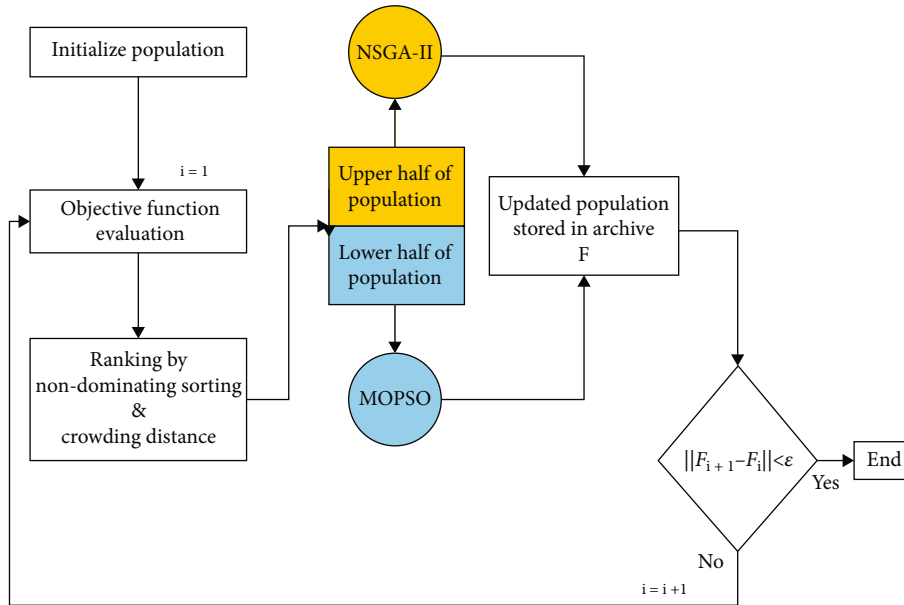FIGURE 3: The Monte Carlo simulation strategy.

FIGURE 4: Mechanism of HNSGAII-MOPSO.

I_b, I_d, and I_H are the beam, diffused, and reflected irradiance, respectively; $\rho_g \in [0.2, 0.7]$ is the albedo; ω is the hour angle; δ denotes the sun's declination angle; ϕ is the latitude; θ_I denotes the incidence angle; θ_z is the panel's zenith angle; γ_s and γ_{SPV} are the sun's and SPV azimuth angles, respectively; thus, $\gamma = \gamma_{spv} - \gamma_s$; α is the altitude angle; and the number of
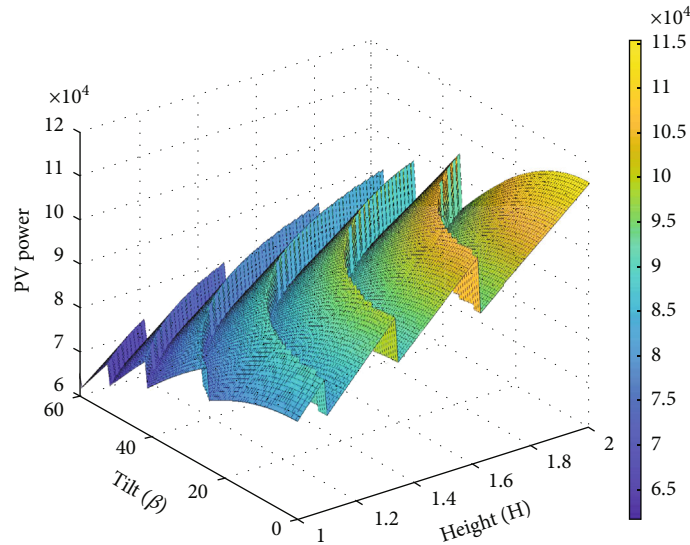
FIGURE 5: The effect of SPV row height (H) on the SPV power.

successive rows is **K**, length of the row is **L**, distance between collector rows is **D**, and height of the row is **H**.

The accuracy of the model (15) depends on the solar geometry (solar angles) depicted by Figure 2. All the angles can be estimated except the azimuth angle (γ) and tilt angle (β), which will be estimated using our optimization approach.

The SPV panel voltage output is given as [49, 54–57]

$$V_{\mathrm{pv}}(t) = N_s \left(\frac{V_{t_1} V_{t_2}}{\Delta V_t}\right) \ln \left\{ \exp\left(-\frac{N_s V_{\mathrm{pv}} + N_p I_{\mathrm{pv}} R_s (N_s/N_p)}{V_{t_2}}\right) \right.$$

$$\cdot \left\{ \left[N_p(I_{\mathrm{sc}} + T_i(T_c - T_f))\left(\frac{I_T}{1000} + 2\right)\left\{ \exp\left[\frac{(N_s V_{\mathrm{oc}} + T_v(T_c - T_f))(N_s \Delta V_t)}{V_{t_1} V_{t_2}}\right] - 1\right\}^{-1} - N_p I_{\mathrm{pv}}\right]$$

$$\cdot \left[N_p(I_{\mathrm{sc}} + T_i(T_c - T_f))\left\{ \exp\left[\frac{N_s(V_{\mathrm{oc}} + T_v(T_c - T_f))(N_s \Delta V_t)}{V_{t_1} V_{t_2}}\right] - 1\right\}^{-1}\right]^{-1} - \left[N_s V_{\mathrm{pv}} + N_p I_{\mathrm{SPV}} R_s\left(\frac{N_s}{N_p}\right)\right]$$

$$\cdot \left[R_p\left(\frac{N_s}{N_p}\right)\left[N_p(I_{\mathrm{sc}} + T_i(T_c - T_f))\left\{ \exp\left[\frac{(N_s V_{\mathrm{oc}} + T_v(T_c - T_f))(\Delta V_t)}{V_{t_1} V_{t_2}}\right] - 1\right\}^{-1}\right]^{-1}\right\} - 1\right\} - N_p I_{\mathrm{pv}} R_s\left(\frac{N_s}{N_p}\right),$$

$$\tag{17}$$

where I_{ph} is the SPV photocurrent, I_{d_1} is the diode 1 current, I_{d_2} is the diode 2 current, I_{R_p} is the shunt current, I_{sc} is the short circuit current, T_i is the temperature coefficient, R_s is the series resistance, R_p is the shunt resistance, T_N is the nominal operating cell temperature, q is the charge of the electron (1.6×10^{-19}C), V_{oc} is the open circuit voltage (V), $n_{1,2}$ is the ideality factors of the diodes, T_v is the temperature coefficient of the open circuit voltage, and k is Boltzmann's constant (1.3805×10^{-23} J/K).

2.3. General Problem Formulation.
The generic Stochastic Multiobjective Optimization Problem (SMOOP) is stated as

$$\underset{\mathbf{X}}{\text{minimize}} \{C_{\mathrm{net}}(\mathbf{x}, \xi), -[P_L(\mathbf{x}, \xi)]\},$$

$$\text{subject to } \left[\frac{\sum_{t=1}^{T}[P_{d,t} - P_{\mathrm{pv},t}(\mathbf{x}, \xi)] \geq 0}{\sum_{t=1}^{T} P_{d,t}}\right] < \alpha, \tag{18}$$
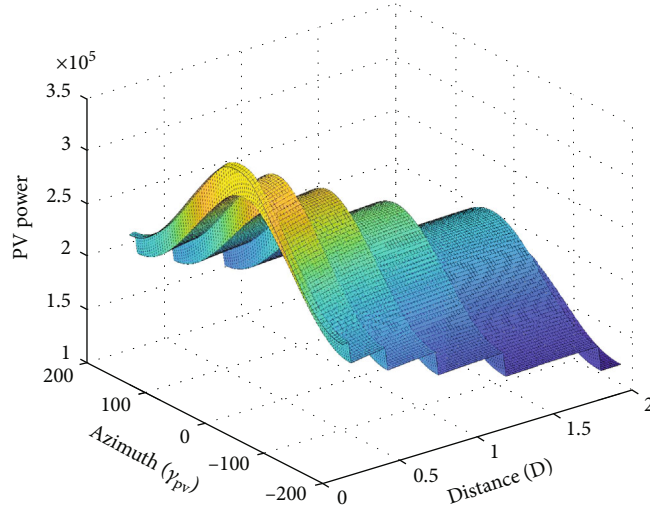
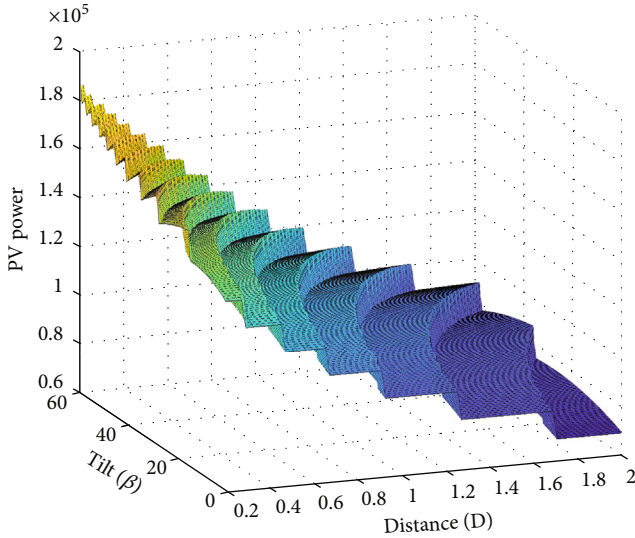FIGURE 6: The effect of SPV azimuth angle (γ_{pv}) variations on the SPV power.

FIGURE 7: Distance (D) effect on SPV power.

$$V^{\min} \leq V_{\text{pv}}(\mathbf{x}, \xi) \leq V^{\max}, \tag{19}$$

$$I^{\min} \leq I_{\text{pv}}(\mathbf{x}, \xi) \leq I^{\max}, \tag{20}$$

$$2R\left[\frac{P_{\text{pv}}(\mathbf{x}, \xi)^2}{V_{\text{pv}}(\mathbf{x}, \xi)^2}\right] < 0.02, \tag{21}$$

$$V_{\text{inv}}^{\min} \leq V_{\text{pv}}(\mathbf{x}, \xi) \leq V_{\text{inv}}^{\max}, \tag{22}$$

$$I_{\text{inv}}^{\min} \leq I_{\text{pv}}(\mathbf{x}, \xi) \leq I_{\text{inv}}^{\max}, \tag{23}$$

$$P_{\text{pv}}(\mathbf{x}, \xi) \leq I_c, \tag{24}$$

$$P_{\text{pv}}(\mathbf{x}, \xi) \leq K_{\text{pv}}, \tag{25}$$

where the decision vector is given by

$$\mathbf{x} = \left[N_s, N_p, I_c, A_w, \theta, \beta, \gamma_{\text{SPV}}, H, K, L, D\right]. \tag{26}$$

The ξ represents the random component.

2.3.1. Constraint Interpretation. In constraint (18), loss of load probability is enforced to meet some desired level of reliability of all generating units. Constraints (19) and (20) ensure that the voltage and current outputs from the inverter must be restrained to avoid large deviation changes during the transition period. That is, the output voltage is stepped up to be more than the grid voltage to ensure power flow from the SPV arrays into the grid, since power flows from the medium voltage (MV) region to the low voltaic (LV) region, but the upper limits of the safe operation grid's voltage must not be exceeded [60].

Usually, the net cable losses for the SPV system must not exceed 2% at all times. Therefore, constraint (21) ensures that the system's wires are optimally sized so that the maximum SPV power loss due to cabling is constrained by the feeder thermal and standard limit of 2% where R is the cable's resistance [61]. This prevents excessive heating and fire due to large current, especially at peak hours.

In constraints (22) and (23), the SPV voltage and current levels must be compatible with the maximum SPV inverter-rated voltage and current, respectively [52]. To maximize SPV power by avoiding higher losses, constraint (24) ensures that the SPV array power is matched with the rated power of the inverter [52]. The amount of SPV power produced per hour cannot exceed the generator [52].

2.3.2. The Limits of the Decision Variables. In this paper, the settings of limits of the decision variables are obtained in the literature and in other industrial settings: $\beta \in [0, 90^0]$, $\gamma_{\text{spv}} \in [-180^0, 180^0]$, $H \in [0.2, 2.0]$, $L \in [5, 40]$, $D \in [0.2, 2.0]$, and $K \in [2, 30]$ were obtained from [50]. The limits of the N_p and N_s are deduced from the study [68]. $\theta \in [0, 90]$ [52].
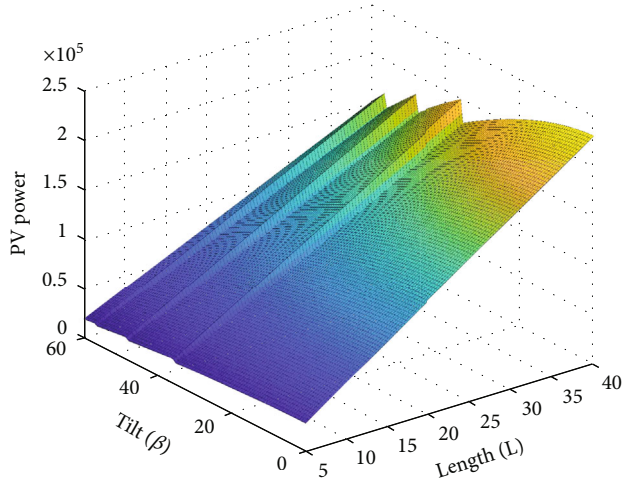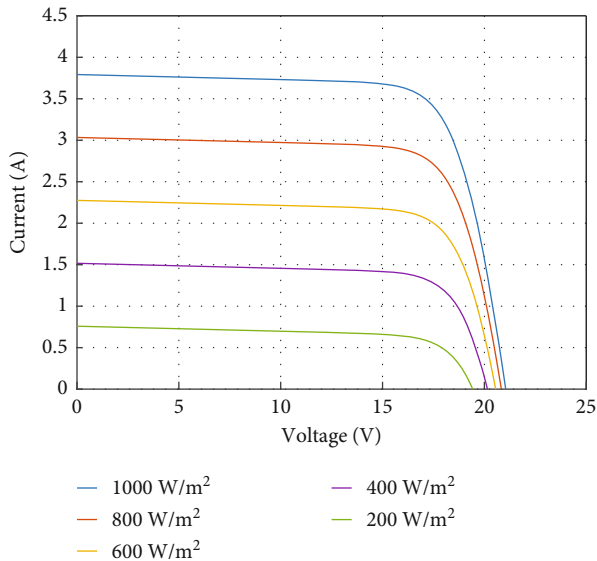
FIGURE 8: Length of SPV row (L) effect on SPV power.

FIGURE 10: Irradiance effect on power.

TABLE 2: Economic characteristics of the SPV system in Ghana.

Parameter	Value	Source
SPV array unit cost	\$100-\$250	[85]
Inverter unit cost	505.05	[86]
SPV installation cost	$40\% \times C_{pv}$	[47]
Cable unit cost	\$16.84	[86]
Grid's electricity tariff	\$0.2	[87]
SPV electricity tariff	$\$(1-2)/Wp$	[88]
SPV unit maintenance cost	\$10/kW/yr	[89]
Inverter's unit maintenance cost	$3\% \times C_{inv}$	[85]
Inverter's unit replacement cost	\$102,565	[90]
Cable's unit replacement cost	\$16.84	[86]
Grid's power (P_g)	3212	
Depreciation rate	$2\% \times IC$	[85]
Inflation rate	5%	[89]
Discount rate	10%	[85]
Project lifetime	25 yrs	[85]
Component's lifetime	5 yrs	[85]

FIGURE 9: Irradiance effect on current and voltage.

The limits of other variables are set according to industrial information in Table 1.

2.4. Solution to the SMOOP. In addressing the uncertainty issue in optimization, different stochastic optimization methods have been proposed in recent years. Among these approaches, the Monte Carlo method (Sample Average Approximation) and Chance Constraint (CC) approaches are the commonest and have many promising real-life applications. However, the main issues with the CC are that it assumes that the randomness follows a bivariant Gaussian distribution and restricts the search space, which consequently makes the problem solution more conservative and lowers its efficiency [47]. Also, similar to solving linear programming, the strategy to solving a nonlinear CC problem is to relax the problem by transforming it into a deterministic problem. However,
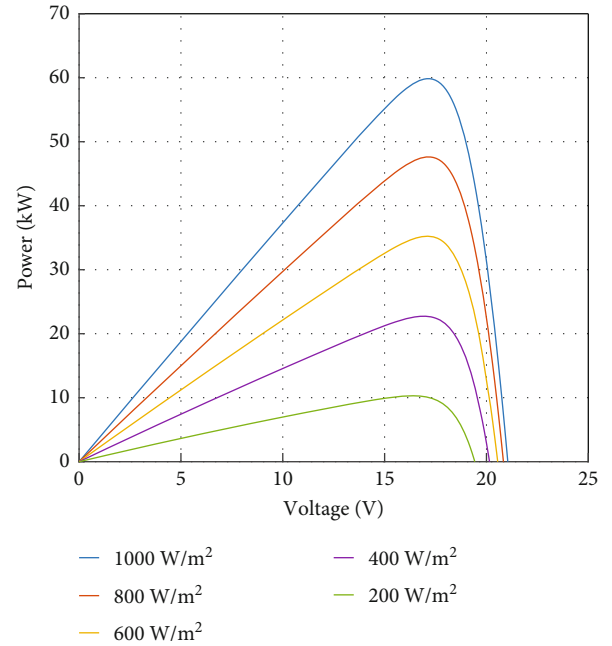
the nonlinear chance-constrained problem is particularly difficult to solve because nonlinear propagation makes it hard to obtain the distribution of output variables even when the distributions of the variables with uncertainty are known [69, 70]. In other words, using the CC will lead to no deterministic equivalent. Several strategies, such as the Sample Average Approximation, are used to approximate the distribution of the output variables [70]. Therefore in this study, in order to find a
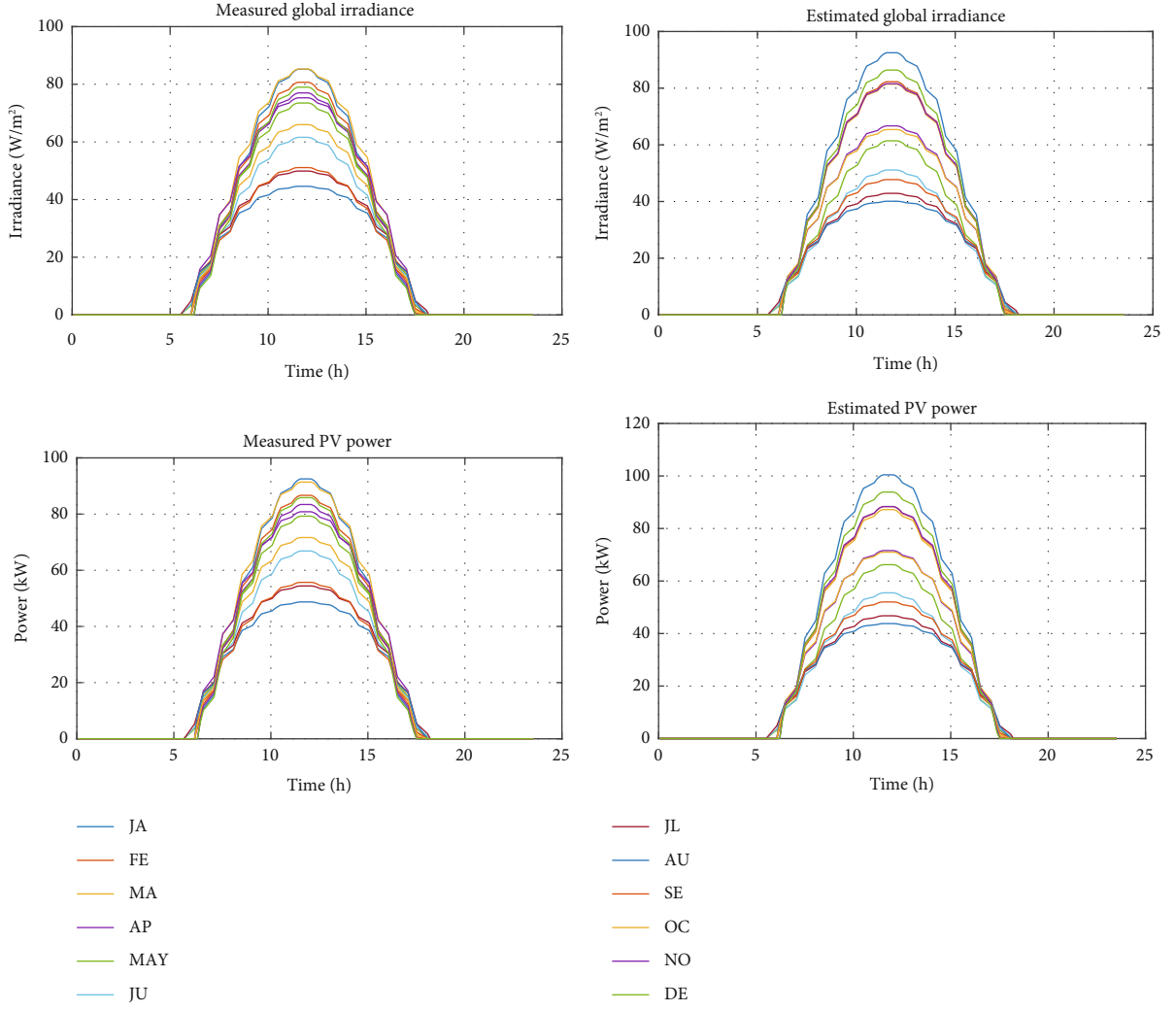
FIGURE 11: Estimated SPV power.

satisfactory stochastically feasible solution for our SMOOP, the Sample Average Approximation (SAA) is employed to handle the uncertainty due to its robustness and effective handling of nonlinear problems.

2.4.1. Sample Average Approximation (SAA). In the Sample Average Approximation, given a random objective function, it could be stated as $F_\nu(\mathbf{K}, \xi)$, for $\nu = 1, 2, \cdots$.

Even if it is possible to demonstrate that $F_\nu(\mathbf{K}, \xi)$ is continuous, differentiable, and convex, such a multidimensional integral might be difficult to comprehend for a given value of $\mathbf{x}$ and even more difficult to optimize [71]. A reasonable way is to boil down the integral to a sum, by sampling N scenarios characterized by realizations ξ_j and probabilities $\pi_j = 1/N$ for $j = 1, 2, \cdots, N$.

Since we cannot directly optimize $F_\nu(\mathbf{K}, \xi)$, its expectation ($\mathbb{E}(F_\nu(\mathbf{K}, \xi))$) must be targeted [71]. Also, according to [72–75], since the feasible set is not deterministic, the principle of constraint in expectation can be used to transform all the random constraints. Thus, the SMOOP is given as

$$\underset{\mathbf{x}}{\text{minimize}} \quad \{\mathbb{E}[C_{\text{net}}(\mathbf{x}, \xi)], -\mathbb{E}[P_L(\mathbf{x}, \xi)]\},$$

$$\text{subject to}\ \mathbb{E}\left[\frac{\sum_{t=1}^{T}\left[P_{d,t} - P_{\text{pv},t}(\mathbf{x}, \xi) \geq 0\right]}{\sum_{t=1}^{T} P_{d,t}}\right] < \alpha,$$

$$V^{\min} \leq \mathbb{E}\left[V_{\text{pv}}(\mathbf{x}, \xi_j)\right] \leq V^{\max},$$

$$I^{\min} \leq \mathbb{E}\left[I_{\text{pv}}(\mathbf{x}, \xi_j)\right] \leq I^{\max},$$

$$\mathbb{E}\left[2R\left(\frac{P_{\text{pv}}(\mathbf{x}, \xi)^2}{V_{\text{pv}}(\mathbf{x}, \xi)^2}\right)\right] < 0.02,$$

$$V_{\text{inv}}^{\min} \leq \mathbb{E}\left[V_{\text{pv}}(\mathbf{x}, \xi_j)\right] \leq V_{\text{inv}}^{\max},$$

$$I_{\text{inv}}^{\min} \leq \mathbb{E}\left[I_{\text{pv}}(\mathbf{x}, \xi_j)\right] \leq I_{\text{inv}}^{\max},$$

$$\mathbb{E}\left[P_{\mathrm{pv},t}\left(\mathbf{x},\xi_j\right)\right] \le I_c,$$

$$\mathbb{E}\left[P_{\mathrm{pv},t}\left(\mathbf{x},\xi_j\right)\right] \le K_{\mathrm{pv}}(t). \tag{27}$$

If we assume realization samples (i.i.d.), $\xi^1, \cdots, \xi^N$ of the random vector N after running the Monte Carlo simulation, then SAA of $F_\nu(\mathbf{K},\xi)$ could be defined as

$$\frac{1}{N}\sum_{\nu=1}^{N} f_\nu(\mathbf{K},\xi_\nu). \tag{28}$$

Applying the law of large numbers gives

$$\frac{1}{N}\sum_{\nu=1}^{N} f_\nu(\mathbf{K},\xi_\nu) \approx \mathbb{E}(F_\nu(\mathbf{K},\xi)). \tag{29}$$

Therefore, the deterministic equivalent of the SMOOP can be given as

$$\underset{\mathbf{X}}{\text{minimize}} \quad \left\{ \frac{1}{N}\sum_{j=1}^{N} C_{\mathrm{net}}(\mathbf{x},\xi), -\left[\frac{1}{N}\sum_{j=1}^{N} P_L(\mathbf{x},\xi)\right] \right\},$$

$$\text{subject to} \frac{1}{N}\sum_{j=1}^{N}\left[\frac{\sum_{t=1}^{T}\left[P_{d,t}-P_{\mathrm{pv},t}(\mathbf{x},\xi)\ge 0\right]\ge 0}{\sum_{t=1}^{T} P_{d,t}}\right] < \alpha,$$

$$V^{\min} \le \frac{1}{N}\sum_{j=1}^{N} V_{\mathrm{pv}}\left(\mathbf{x},\xi_j\right) \le V^{\max},$$

$$I^{\min} \le \frac{1}{N}\sum_{j=1}^{N} I_{\mathrm{pv}}\left(\mathbf{x},\xi_j\right) \le I^{\max},$$

$$\frac{2R}{N}\sum_{j=1}^{N}\left[\frac{P_{\mathrm{pv}}(\mathbf{x},\xi)^2}{V_{\mathrm{pv}}(\mathbf{x},\xi)^2}\right] < 0.02,$$

$$V_{\mathrm{inv}}^{\min} \le \frac{1}{N}\sum_{j=1}^{N} V_{\mathrm{pv}}\left(\mathbf{x},\xi_j\right) \le V_{\mathrm{inv}}^{\max},$$

$$I_{\mathrm{inv}}^{\min} \le \frac{1}{N}\sum_{j=1}^{N} I_{\mathrm{pv}}\left(\mathbf{x},\xi_j\right) \le I_{\mathrm{inv}}^{\max},$$

$$\frac{1}{N}\sum_{j=1}^{N} P_{\mathrm{pv}}\left(\mathbf{x},\xi_j\right) \le I_c,$$

$$\frac{1}{N}\sum_{j=1}^{N} P_{\mathrm{pv}}\left(\mathbf{x},\xi_j\right) \le K_{\mathrm{pv}}(t). \tag{30}$$

We now discuss the multiobjective optimization method to solve this deterministic problem.

The general stochastic design approach is summarized by Figure 3.

2.4.2. Multiobjective Optimization Approaches. In Multiobjective Optimization Problems (MOOP), the objective func-

Table 3: Household appliance data.

Appliance	P_{sat}	W_n (W)	W_{stan}	f	t_{cycle}
Microwave oven	0.93	1500	0	7.5	5
Refrigerator 1	1.0	110	8.10	40.5	12
Refrigerator 2	0.31	110	8.10	40.5	12
Coffee maker	0.37	1000	0	1.12	6
Clothes washer	1.0	1200	0	0.75	54
TV 1	1.0	105	4	1.95	90
TV 2	0.21	83	4	0.28	60
Air conditioning	0.93	1300	0	2.36	120
Lighting	1.0	120	0	18	30

Months

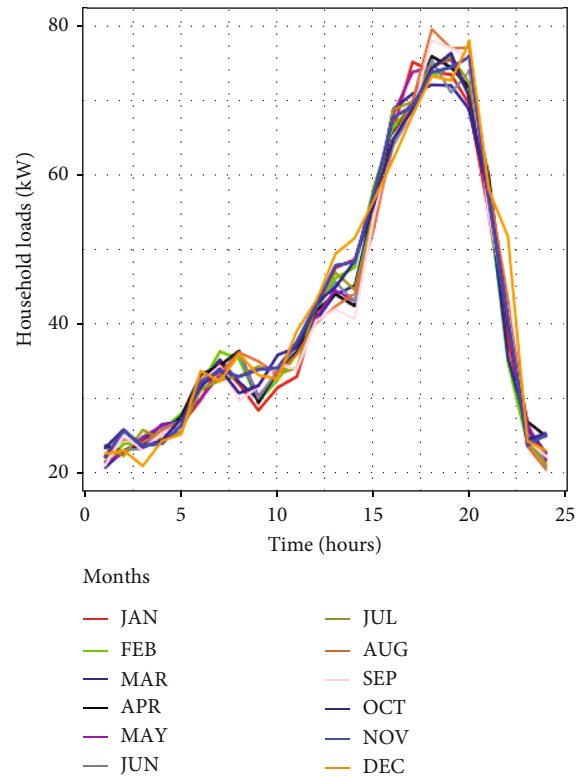|	
— JAN	— JUL
— FEB	— AUG
— MAR	— SEP
— APR	— OCT
— MAY	— NOV
— JUN	— DEC

Figure 12: Household load demand.

tions frequently conflict. This leads to a large number of optimal solutions that are called nondominated or Pareto optimal solutions.

Theorem 1. *For $y^* \in \mathbb{S}$, the set y^* and its corresponding $f(y^*)$ are said to be a nondominated solution if and only if no other feasible solution $y \in \mathbb{S}$ exists s.t. $f_j(y) \le f_j(y^*), \forall k$ and $f_j(y) < f_j(y^*)$ for at least one objective.*

According to [76–78], among the multiobjective methods, Multiobjective Evolutionary Algorithms (MOEAs) seem to be more promising. They can hunt for solutions nearer to the actual Pareto fronts or be widely dispersed
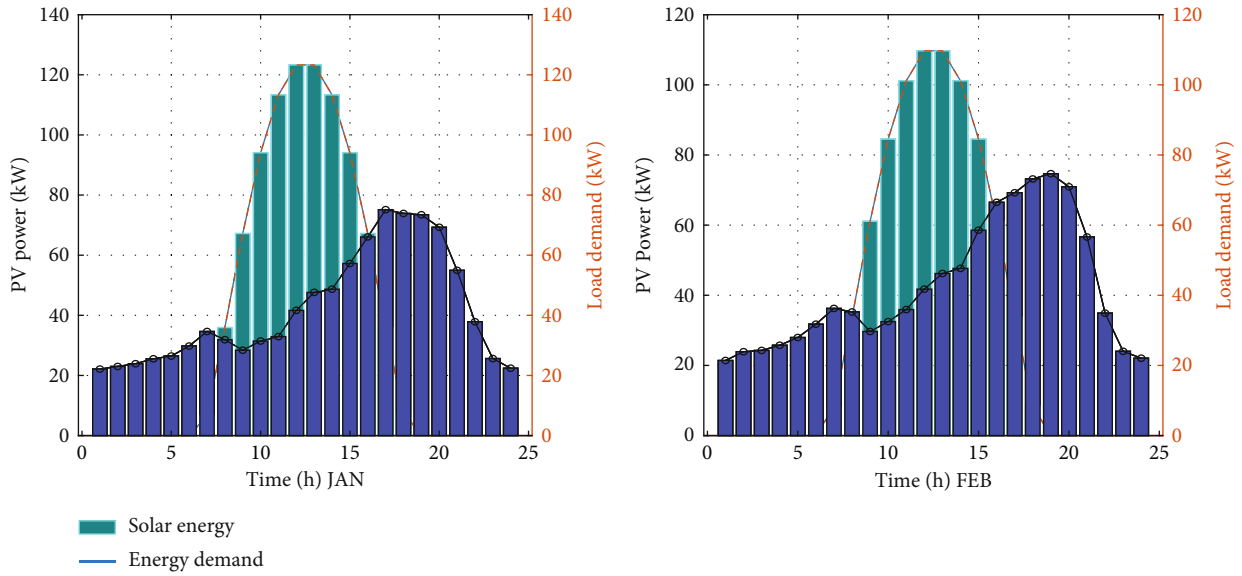
FIGURE 13: Comparison of load demand and SPV power produced from January to February.
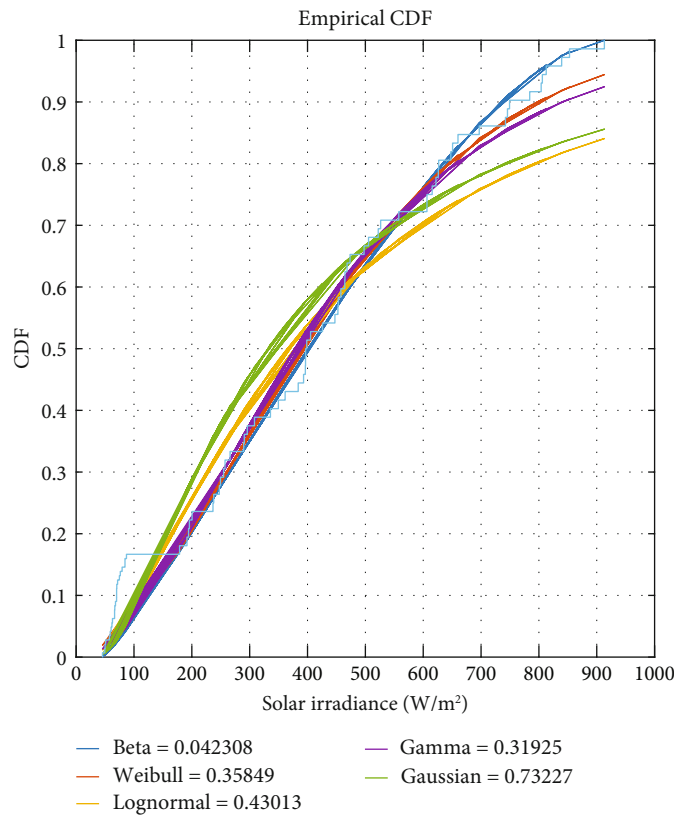

FIGURE 14: Comparison of simulated and actual CDFs.

enough to cover the complete Pareto front range or handle discontinuous functions, nonconvexity, etc.

We note that several standard MOEAs have been successfully used in numerous MOOP applications for decades. Key among them are the Strength Pareto Evolutionary Algorithm-2 (SPEA-2), Pareto Envelope-based Selection Algorithm II (PESA-II), Nondominated Sorting Genetic

Algorithm II (NSGA-II), and Multiobjective Particle Swarm Optimization (MOPSO).

Convergence, diversity preservation, and execution time are the factors used to decide the superiority of these algorithms [79, 80]. To determine the algorithm that would solve this problem better, we undertake a thorough comparative analysis in this paper.
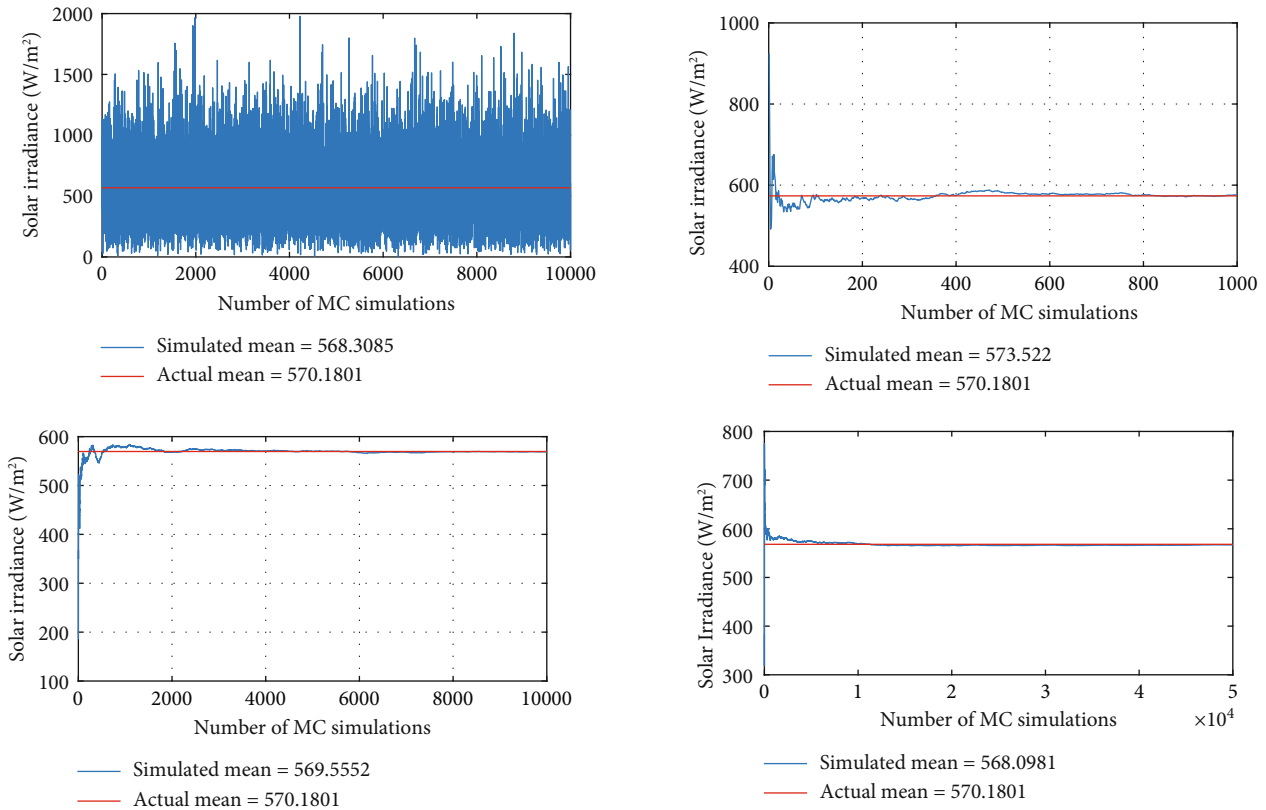
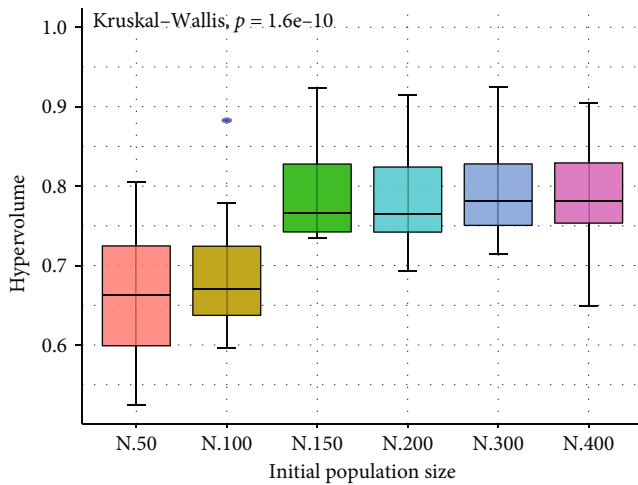Figure 15: Simulation of solar irradiance with Monte Carlo simulations.

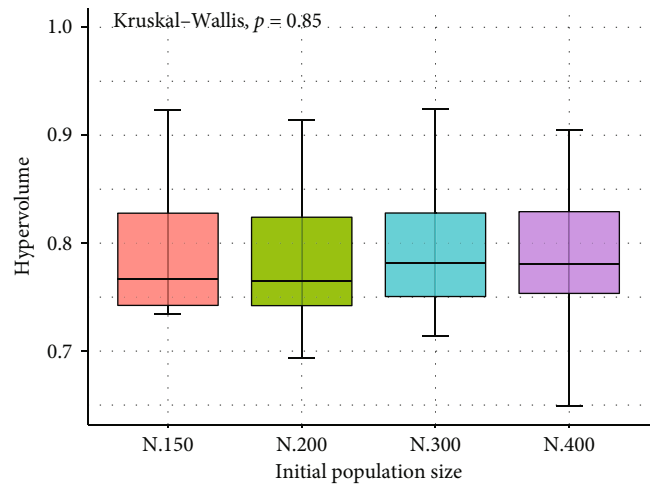Figure 16: Comparison of six initial populations.

Figure 17: Comparison of higher initial populations.

2.4.3. Hybrid Multiobjective Optimization Methods.

Generally, most MOEAs get stuck in the local optimum when dealing with highly complex problems (nonlinear, nonconvex, nonsmooth, etc.). While some algorithms more thoroughly explore the search space and slowly converge, others thoroughly exploit but fail to discover the best solution [81]. Therefore, creating a hybrid algorithm is necessary to maintain the proper balance between exploration and exploitation. This study has applied a Hybrid NSGA-II and

MOPSO (HNSGAII-MOPSO) algorithm to solve the deterministic equivalent problem. During the rank-based solution search, the population is partitioned into two. The exploration mechanism was performed by the NSGA-II using the upper half of the population. Adjusting the MOPSO to exploit the other part of the population efficiently was accomplished by maximizing the learning coefficient of individuals, minimizing the global learning coefficient, and applying an adaptive mutation operator. The details of this

TABLE 4: Parameters used in the six standard MOEAs.

Parameter	NSGA-II	MOPSO	PESA-II	SPEA-2	NSGAII-MOPSO
Population size	150	150	150	150	150
Maximum iteration	100	100	100	100	100
Repository size	—	100	100	100	50
Mutation rate	—	0.1	—	—	0.1
Mutation step size	0.02	—	—		0.02
Crossover percentage	0.7	—	0.5	0.7	0.7
Mutation percentage	0.4	—	0.5	0.3	0.4
Inertia weight	—	0.5	—		0.5
Personal learning coefficient	—	1	—	—	4
Global learning coefficient	—	2	—	—	1
Inflation rate	—	0.1			0.1
Inertia-damping rate	—	0.99	—	—	0.99
Leader pressure	—	2	—	—	2
Deletion selection pressure	—	2	—	—	2
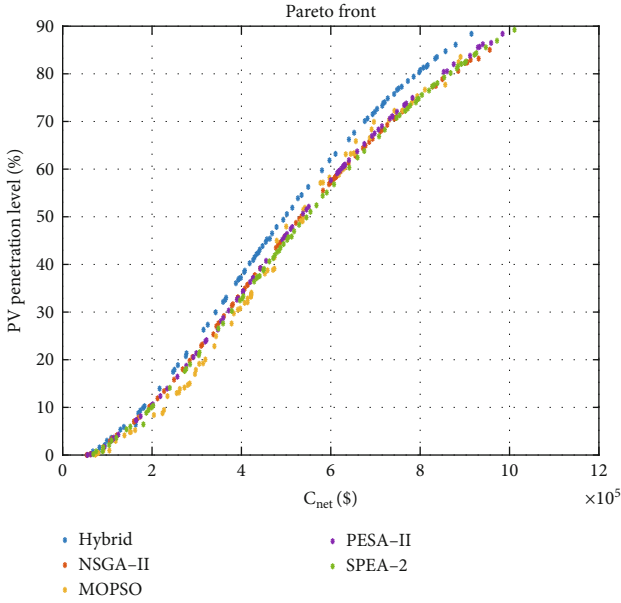
FIGURE 18: Comparison of Pareto fronts of five MOEAs.

FIGURE 19: The algorithm performance based on hypervolume indicator.

algorithm can be found in [81], and its mechanisms are shown in Figure 4.

2.5. Performance Assessment with Hypervolume Metric. For nonlinear problems, the solution techniques often do not have convergence proofs [80]. Nevertheless, there are numerous measures for convergence and diversity preservation. The following papers go into detail on each one [76, 79, 80, 82, 83]. Among the metrics, hypervolume is used in this paper since, according to a thorough review by [83], it is the most frequently used in the literature. It simultaneously evaluates proximity and diversity, and the higher the value, the better the approximation (signifying better solution spread and convergence).

Given the Pareto front approximation $\mathbf{S}$ and a reference point $r \in \mathbb{R}^m$ s.t. $\forall z \in S$, $z \prec r$, the hypervolume indicator is given by [84]

$$H(S, r) = \lambda_m \left(\bigcup_{z \in S} [z ; r] \right), \tag{31}$$

where λ_m is the m-dimensional Lebesgue measure.

3. Simulations, Results, and Discussions

In this study, our design approach is a simulation-based optimization technique. The optimization generates the optimal result, and the simulation handles the randomness.

3.1. Simulations. In validating the modelling strategy, an on-grid HESS considering the SPV and grid electricity is

TABLE 5: Comparison of the hybrid algorithm with four other standard MOEAs based on hypervolume (convergence, diversity) and execution time.

Statistic	Hypervolume					Execution time (s)				
	NSGA-II	MOPSO	SPEA-2	PESA-II	Hybrid	NSGA-II	MOPSO	SPEA-2	PESA-II	Hybrid
Mean	0.7395	0.6993	0.5884	0.6281	0.7884	421.4	436.9	453.4	457.7	425.1
Median	0.7134	0.6916	0.5664	0.6405	0.7663	426.0	436.9	457.8	457.7	422.8
Min	0.6258	0.6057	0.5346	0.5308	0.7346	399.0	406.3	421.4	422.6	401.8
Max	1.0031	0.8711	0.7232	0.7201	0.9232	451.1	459.0	487.3	483.2	458.0

constructed for a standard household. The SPV array mounted on the ground, coupled to a combiner box, and a string inverter make up the grid-connected system. The electrical utility grid receives the excess energy that the solar owner does not use and distributes it to other users. The HESS simulations and optimization modelling are done in MATLAB and R environments using an i5 core processor running at 2.67 GHz and 4 GB of RAM.

3.1.1. Impacts of Decision Variables on SPV Power. One set of variables that we control to optimize the objectives are the SPV layout parameters: number of successive rows (**K**), length of the row (**L**), distance between collector rows (**D**), and height of the row (**H**). Figures 5–8 show the relationship between the SPV power and these field variables. This helps validate the modelling strategy as various regions with high energy levels are displayed. After optimization, the most optimal solution will be expected to fall within these regions.

In Figure 5, it can be seen that the maximum power falls around a tilt angle of 25°–30° and a height of 1.8 m–2.0 m. In Figure 6, the maximum power occurs at distance 0.4 m–0.6 m and an azimuth angle of almost zero. This is in line with the findings in [50] that when close to the equator, the azimuth angle is approximately zero. In Figure 7, the amount of power decreases as the distance between the successive panels widens. This is due to the fact that at a higher distance, few number panels could be installed within the area. In reality, the longer the length of an array row, the larger the power obtained. This is clearly demonstrated by Figure 8.

3.1.2. Irradiance Effects on Voltage and Current. We analyze the impact of irradiance on voltage and current using the I-V characteristic curves at various values of solar irradiance. These are shown by Figures 9 and 10.

It can be observed in Figure 9 that the current increases quasilinearly as irradiance, and the voltage (V_{spv}) is in a logarithmic pattern with irradiance. Also, from Figure 10, the maximum power increases faster than the solar irradiance, and this implies that the SPV efficiency is at its best, especially at a higher level of irradiance.

3.2. The Model Input Data. The modelling validation is carried out with the following hourly data: solar irradiance, energy consumption profiles, and economic characteristics of the SPV system as shown in Tables 1 and 2. Figure 11 shows the simulated irradiation quantity with the respective
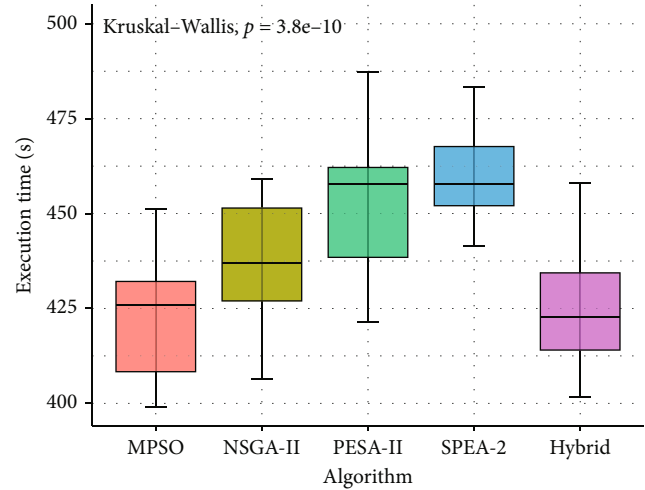

FIGURE 20: Comparison of algorithms by execution time.

power. It was calculated using measurements of solar irradiance on the horizontal surface taken at KNUST (latitude 6.6732°). The choice of an hourly time step is predicated on the idea that changes in the RES have little impact over the course of one hour.

The cost of the components is estimated based on what is currently being offered on the market.

The hourly energy consumption data was estimated using a robust probabilistic approach called the bottom-up method, whose theoretical details can be found in [3, 59, 91]. The consumption profiles in Table 3 are used in the simulation.

The simulated hourly load demand for each month in the year is shown in Figure 12.

Figure 13 displays the specifics of the SPV power and the energy demand for a few months to keep things simple. The grid power is used to address the energy shortage. This analysis provides numerous suggestions on blackout hours throughout the months, and it assists the designer in doing a thorough reliability assessment for the HESS.

Fitting historical weather data to a suitable probability distribution helps in modelling the randomness in solar irradiance, and the expected values are then calculated by the Monte Carlo simulation using the distribution outputs. In this paper, to fit the randomness effect in irradiance, the cumulative distribution functions (CDFs) of five standard probability distribution functions—Weibull, beta, lognormal, gamma, and Gaussian—were used. By comparing the output of each distribution with the actual data calculated,

Table 6: Comparison of the hybrid algorithm with four other standard MOEAs based on the accuracy of the SPV penetration level and net present cost.

Statistic	SPV penetration level (%)					Net present cost ($)				
	NSGA-II	MOPSO	SPEA-2	PESA-II	Hybrid	NSGA-II	MOPSO	SPEA-2	PESA-II	Hybrid
Mean	43.78455	38.8779	50.8815	52.136	45.8443	493,377	458,730	10,554,312	377,114	479,029
Median	45.63694	34.0536	51.7054	46.969	44.7288	495,552	422,391	8255,646	284,127	454,491
Min	0.01313	0.3874	0.7716	3.673	0.1812	53,866	76,311	75,410	74,525	61,950
Max	85.03154	83.55515	87.0677	85.9120	88.3962	955,711	890,418	46,176,673	1,255,801	914,834

the beta with RMSE = 0.042308 outperformed the rest based on the RMSE analysis. The result is illustrated in Figure 14.

Monte Carlo simulations for different samples were run. The results in Figure 15 show that even at 10,000 simulations, the simulated mean of solar irradiance approaches the actual mean of the data.

3.3. The Optimization Module. These MOEAs rely on specific parameters and functions, whose varying levels have impacts on their speed, diversity, and convergence capabilities. We perform numerous runs of different parameter combinations, and the best set is utilized to solve the problem. This allows us to determine the ideal settings for each MOEA which could enhance the execution time, the convergence, and the capacity to create a diverse solution. For instance, six distinct population sizes—50, 100, 150, 200, 300, and 400—were examined in the HNSGAII-MOPSO and evaluated using running time and the hypervolume indicator. For each value, each algorithm was run 40 times. The result in Figure 16 shows the presence of instability when the population size is between 50 and 100.

This demonstrates unequivocally that the algorithm occasionally ends up in suboptimal solutions because of their lower hypervolume indices.

When there are 150 or more people in the population, the optimal value is steady, and changing population sizes will result in equally effective solutions. Figure 17 shows that there is no discernible difference between the hypervolume indicator when the population size is 150 or higher, which could lead the HNSGAII-MOPSO to a better and more effective solution.

The execution time rose as the population size increased since it is almost linearly correlated with population size. We used the following parameters in the MOEAs.

A similar analysis is carried out for each parameter in each method. Although each algorithm has its own set of operations and search techniques, the algorithms are all based on the same maximum number of iterations, population size, and archive size to make the algorithms contrast. Table 4 summarizes the best parameters.

3.3.1. Comparison of the Proposed Mechanism with Other Methods. In this section, we compare the accuracy, convergence, and execution time of the proposed method with other existing approaches. These analyses are carried out on the Pareto optimal solution obtained. Since all the five MOEAs are heuristic search techniques, some uncertainty
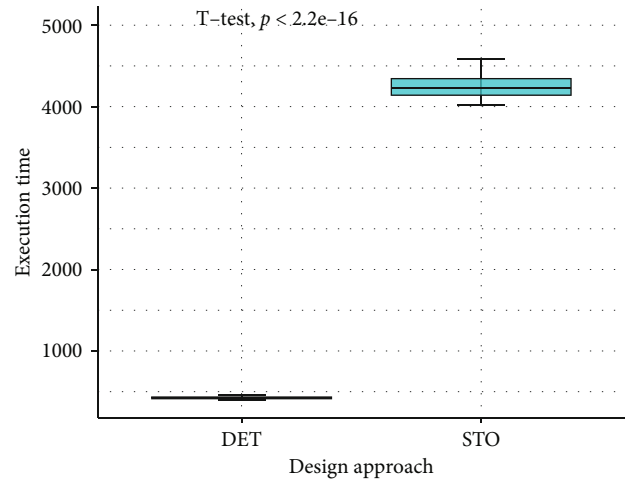

Figure 21: Comparison of design methodology based on execution time.

exists in their results. Therefore, the procedure is performed 40 times independently to remove the contingency, and the comparison analysis is based on averaged recordings displayed in Figure 18. Nonparametric tests were used to examine the significance of median variations between algorithms and designs. Nonparametric tests, in contrast to parametric tests, are appropriate for data that are not normally distributed and assume a flexible or no distribution [92]. In this study, the significance levels in the median of the hypervolume and the execution times of each algorithm are tested using the Kruskal-Wallis nonparametric test, which is an analogous one-way ANOVA. The Mann-Whitney-Wilcoxon test is also used to determine whether the two samples' medians differ. From Figure 19, it can be observed that the differences in the hypervolume are statistically significant according to the Kruskal-Wallis test. Also, according to Table 5, the HNSGAII-MOPSO has higher hypervolume values, and the NSGA-II, MOPSO, SPEA-2, and, finally, PESA-II follow in that order. Also, from Figure 20 and Table 5, it can be seen that the HNSGAII-MOPSO is more time-efficient. Again, in Table 6, the HNSGAII-MOPSO has better mean and median values in both objectives as compared to the other four MOEAs. This suggests that the HNSGAII-MOPSO algorithm has a better accuracy and faster convergence capacity, which causes its solution to be more evenly distributed and closer to the approximate Pareto front. It could be inferred that the PESA-II tends to get stuck in the local optimum due to its worst hypervolume values.

TABLE 7: The most optimal solution.

P_L (%)	C_{net} ($)	I_c	$R_c + G_c$	M_c
81.4852	901,913.42	721,530.736	126,267.8788	54,114.8052

TABLE 8: The most optimal design.

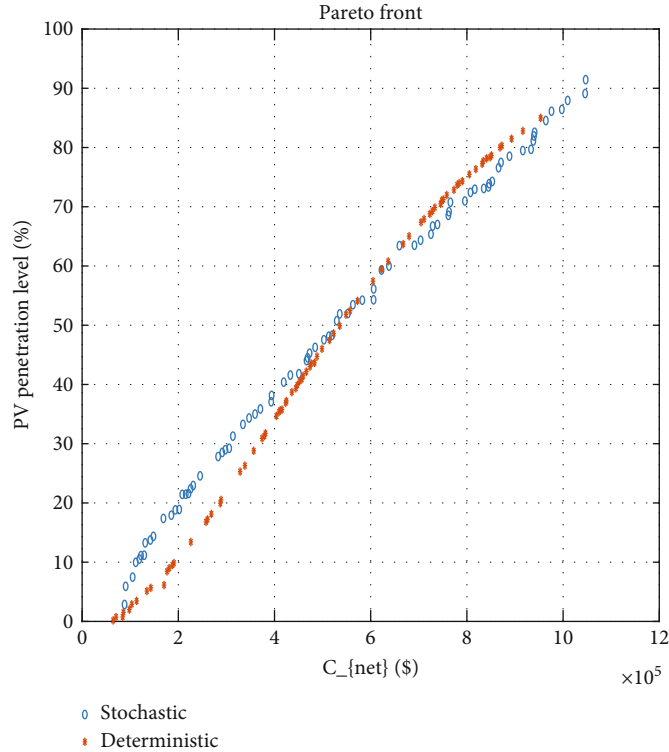| N_s	N_p	I_c (kW)	A_w (AWG)	θ	β	γ_{pv}	H	K	L	D
6	4	3.5	1.3	0.9^0	26.2^0	0.0005^0	2 m	20 m	40 m	0.42 m

FIGURE 22: Comparison of stochastic and deterministic solutions.

Using the predetermined average irradiance and the results of the Monte Carlo simulation, we approach the problem in both deterministic and stochastic ways. The solutions are shown in Figure 21. The cost breakdown has been provided, so the DM will clearly understand the design's fixed and recurring costs.

3.4. Post-Pareto Front Analysis and Sensitivity Analysis.
It would be difficult for the decision-maker to select the most optimal solution from the set of 80 nondominated solutions. Multiple-criterion decision-making techniques that are resilient and crucial must be used in this situation. The study [41] contains a thorough and in-depth evaluation of multiple-criterion decision-making techniques for MOOP. To improve the decision-making process, the Technique for Order of Preference by Similarity to Ideal Solution (TOPSIS), a post-Pareto analysis technique, was used in this study. More information on TOPSIS can be found in [93].

This approach was chosen because it is straightforward and reliable in the decision-making process [41].

After the post-Pareto front analysis, the most optimal solution and the decision variable are shown in Tables 7 and 8.

3.5. Discussion of Results.
Figure 22 shows the outcomes of the two designs, and Figure 21 shows that the stochastic design takes almost 18 times as long to execute as the deterministic case. The HNSGAII-MOPSO performs better on the deterministic MOOP than on the stochastic case. However, from Figure 23, the level of reliability in the stochastic case, on the other hand, is much higher than in the deterministic case, implying that the stochastic design would assist decision-makers in selecting solutions that are evaluated in scenarios that are closer to the real-life situation than assuming constant irradiance in the deterministic design. Also, the cost for the stochastic scenario is also seen to be lower than that for the deterministic case.
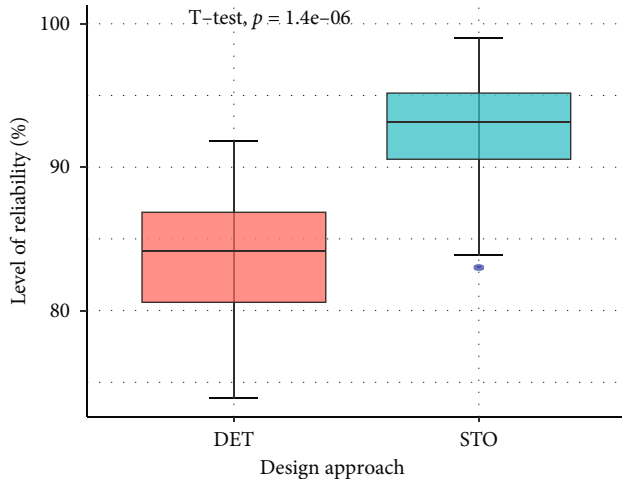
FIGURE 23: Comparison of design methodology based on system reliability.

TABLE 9: Characteristics examined in the sensitivity analysis.

Parameters	Worst case (-10%)	Best case (+10%)
SPV efficiency (15%)	P_L, -9.303%	P_L, +9.298%
Interest rate (5%)	C_{net},-3.41%	C_{net}, +3.391%
SPV capital cost	C_{net}, -7.67%	C_{net}, +9.291%

The most optimal solution displayed by Table 7 implies that the system designers should make the decision given by the Table 8 that yields a maximum SPV penetration level of 81.4852% and a cost of $901,913.42 without collapsing the grid's operational limitations. From Figures 5–8, we can conclude that the optimization procedure was able to extract the desired variables since each of these field variables falls within the regions with maximum SPV power.

The findings of the sensitivity analysis are shown in Table 9, and it is clear that the initial capital significantly influences the design goals.

4. Conclusion and Recommendations

This study proposes a novel stochastic multiobjective optimization design methodology for selecting and controlling the maximum allowable penetration level of Solar Photovoltaic resources at a minimum cost without violating the grid's operational constraints. To attain a quality solution, a detailed comparative analysis of five cutting-edge MOEAs by hypervolume measure, run time, and the nonparametric statistical test was performed. The results proved that the HNSGAII-MOPSO had a better hypervolume measure and was more time-efficient. Also, in Table 6, the HNSGAII-MOPSO has better mean and median values in both objectives as compared to the other four MOEAs. These suggest that the HNSGAII-MOPSO algorithm has a better accuracy and faster convergence capacity, which causes its solution to be more evenly distributed and closer to the approximate Pareto front. The final solution showed that with given grid

characteristics, the maximum allowable SPV penetration level required to ensure full electricity coverage without violating the grid's operational constraints was 81.4852% at the cost of $901,913.42. Even under fluctuating weather conditions, the modelling strategy can help to optimally design the HESS to ensure full energy coverage at an affordable cost. Again, from the system's reliability analysis, it can be inferred that the HNSGAII-MOPSO works better on the deterministic MOOP than in the stochastic case. However, the stochastic design was more reliable and cost-effective. Minor variations in the capital cost could result in a sizable change in the design results according to sensitivity analysis used to examine the impact of changes in the economic factors on the optimal solution. It is recommended that the stochasticity in the economic characteristics should be captured in future studies. Also, additional renewable energy sources such as the wind could be included in the design process.

Data Availability

All the data used in the study will be made available upon request.

Conflicts of Interest

The authors declare that they have no conflicts of interest.

Acknowledgments

References

[1] A. Bouaouda and Y. Sayouti, "Hybrid meta-heuristic algorithms for optimal sizing of hybrid renewable energy system: a review of the state-of-the-art," *Archives of Computational Methods in Engineering*, vol. 29, no. 6, pp. 4049–4083, 2022.

[2] M. I. Hlal, V. K. Ramachandaramurthya, S. Padmanaban et al., "NSGA-II and MOPSO based optimization for sizing of hybrid PV-wind-battery energy storage system," *International Journal of Power Electronics and Drive Systems*, vol. 10, no. 1, p. 463, 2019.

[3] A. Abubakar, R. N. Borkor, and P. Amoako-Yirenkyi, "Stochastic optimal design of household-based hybrid energy supply systems using sample average approximation," *Mathematical Problems in Engineering*, vol. 2022, Article ID 9021413, 19 pages, 2022.

[4] E. A. Sharew, H. A. Kefale, and Y. G. Werkie, "Power quality and performance analysis of grid-connected solar PV system based on recent grid integration requirements," *International Journal of Photoenergy*, vol. 2021, Article ID 4281768, 14 pages, 2021.

[5] L. Ji, Z. Liu, Y. Wu, and G. Huang, "Techno-economic feasibility analysis of optimally sized a biomass/PV/DG hybrid system under different operation modes in the remote area," *Sustainable Energy Technologies and Assessments*, vol. 52, article 102117, 2022.

[6] L. Ali, S. M. Muyeen, H. Bizhani, and M. G. Simoes, "Game approach for sizing and cost minimization of a multi-microgrids using a multi-objective optimization," in *2021 IEEE*

Green Technologies Conference (GreenTech), pp. 507–512, Denver, CO, USA, 2021.

[7] T. Adefarati, G. Sharma, A. K. Onaolapo et al., "Optimal design and techno-economic analysis of a grid-connected photovoltaic and battery hybrid energy system," *International Journal of Engineering Research in Africa*, vol. 60, pp. 125–154, 2022.

[8] F. Xuan, M. Han, A. Kumar, S. Vishwakarma, N. Kannan, and R. Jain, "Optimization of grid-connected photovoltaic power generation technology based on nonlinear back-stepping controller," *Mathematical Problems in Engineering*, vol. 2022, Article ID 2713874, 8 pages, 2022.

[9] M. A. Basit, S. Dilshad, R. Badar, and S. M. Sami ur Rehman, "Limitations, challenges, and solution approaches in grid-connected renewable energy systems," *International Journal of Energy Research*, vol. 44, no. 6, pp. 4132–4162, 2022.

[10] A. K. Hamid, N. T. Mbungu, A. Elnady, R. C. Bansal, A. A. Ismail, and M. A. AlShabi, "A systematic review of grid-connected photovoltaic and photovoltaic/thermal systems: benefits, challenges and mitigation," *Energy & Environment*, vol. 33, no. article 0958305X221117617, pp. 1–40, 2022.

[11] C. Chen, H. Liu, Y. Xiao, F. Zhu, L. Ding, and F. Yang, "Power generation scheduling for a hydro-wind-solar hybrid system: a systematic survey and prospect," *Energies*, vol. 15, no. 22, p. 8747, 2022.

[12] M. Kumar, "Social, economic, and environmental impacts of renewable energy resources," in *Wind Solar Hybrid Renewable Energy System*, vol. 1, IntechOpen, London, UK, 2020.

[13] H. K. Pujari and M. Rudramoorthy, "Optimal design, techno-economic and sensitivity analysis of a grid-connected hybrid renewable energy system: a case study," *International Journal of Emerging Electric Power Systems*, vol. 23, 2022.

[14] I. De Mel, O. V. Klymenko, and M. Short, "Complementarity reformulations for the optimal design of distributed energy systems with multiphase optimal power flow," http://arxiv.org/abs/2204.12963.

[15] E. Zhao, Y. Han, X. Lin, E. Liu, P. Yang, and A. S. Zalhaf, "Harmonic characteristics and control strategies of grid-connected photovoltaic inverters under weak grid conditions," *International Journal of Electrical Power & Energy Systems*, vol. 142, article 108280, 2022.

[16] M. A. Khan, A. Haque, V. B. Kurukuru, and M. Saad, "Islanding detection techniques for grid-connected photovoltaic systems-a review," *Renewable and Sustainable Energy Reviews*, vol. 154, article 111854, 2022.

[17] R. Khezri, A. Mahmoudi, and H. Aki, "Optimal planning of solar photovoltaic and battery storage systems for grid-connected residential sector: review, challenges and new perspectives," *Renewable and Sustainable Energy Reviews*, vol. 153, article 111763, 2022.

[18] Q. Peng, A. Sangwongwanich, Y. Yang, and F. Blaabjerg, "Grid-friendly power control for smart photovoltaic systems," *Solar Energy*, vol. 210, pp. 115–127, 2020.

[19] W. A. Salem, W. Gabr Ibrahim, A. M. Abdelsadek, and A. A. Nafeh, "Grid connected photovoltaic system impression on power quality of low voltage distribution system," *Cogent Engineering*, vol. 9, no. 1, article 2044576, 2022.

[20] Y. Yang, F. Blaabjerg, H. Wang, and M. G. Simões, "Power control flexibilities for grid-connected multi-functional photovoltaic inverters," *IET Renewable Power Generation*, vol. 10, no. 4, pp. 504–513, 2016.

[21] A. Ghaedi, A. Abbaspour, M. Fotuhi-Friuzabad, and M. Parvania, "Incorporating large photovoltaic farms in power generation system adequacy assessment," *Scientia Iranica*, vol. 21, no. 3, pp. 924–934, 2019.

[22] Z. Xu, S. Tao, H. Fan, J. Sun, and Y. Sun, "Power limit control strategy for household photovoltaic and energy storage inverter," *Electronics*, vol. 10, no. 14, p. 1704, 2021.

[23] M. Li, S. Shu, Y. Wang et al., "Analysis and improvement of large-disturbance stability for grid-connected VSG based on output impedance optimization," *IEEE Transactions on Power Electronics*, vol. 37, no. 8, pp. 9807–9826, 2022.

[24] S. Nasef, A. Hassan, H. ElMadany, M. Zahran, M. EL-Shaer, and A. Abdelaziz, "Optimal power management and control of hybrid photovoltaic-battery for grid-connected doubly-fed induction generator based wind energy conversion system," *International Journal of Renewable Energy Research*, vol. 12, 2022.

[25] P. Denholm and R. Margolis, *Energy storage requirements for achieving 50% solar photovoltaic energy penetration in California*, National Renewable Energy Lab.(NREL), Golden, CO (United States), 2016.

[26] S. Bacha, D. Picault, B. Burger, I. Etxeberria-Otadui, and J. Martins, "Photovoltaics in microgrids: an overview of grid integration and energy management aspects," *IEEE Industrial Electronics Magazine*, vol. 9, no. 1, pp. 33–46, 2015.

[27] E. Rakhshani, K. Rouzbehi, A. J. Sánchez, A. Cabrera Tobar, and E. Pouresmaeil, "Integration of large scale PV-based generation into power systems: a survey," *Energies*, vol. 12, no. 8, p. 1425, 2019.

[28] M. S. Giridhar, K. R. Rani, P. S. Rani, and V. Janamala, "Mayfly algorithm for optimal integration of hybrid photovoltaic/battery energy storage/D-STATCOM system for islanding operation," *International Journal of Intelligent Engineering and Systems*, vol. 15, pp. 225–232, 2022.

[29] K. Anoune, A. Laknizi, M. Bouya, A. Astito, and A. B. Abdellah, "Sizing a PV-wind based hybrid system using deterministic approach," *Energy Conversion and Management*, vol. 169, pp. 137–148, 2018.

[30] M. Seruca, A. Mota, and D. Rodrigues, *Solving the economic scheduling of grid-connected microgrid based on the strength Pareto approach*, University Library of Munich, 2019.

[31] L. Xiong, M. Nour, and M. Shahin, "Harmonic analysis of high penetration level of photovoltaic generation in distribution network and solution studies," in *2019 8th International Conference on Modeling Simulation and Applied Optimization (ICMSAO)*, pp. 1–5, Manama, Bahrain, 2019.

[32] R. Khezri, A. Mahmoudi, and H. Aki, "Multi-objective optimization of solar PV and battery storage system for a grid-connected household," in *2020 IEEE International Conference on Power Electronics, Drives and Energy Systems (PEDES)*, pp. 1–6, Jaipur, India, 2020.

[33] H. Arbabi, *Optimal design of wind-solar-battery off-grid hybrid system using metaheuristic algorithm for Mile Nader region, [Ph.D. thesis]*, University of Zabol, 2021.

[34] W. Nemouchi, Y. Amrane, and H. Nemouchi, "Optimal Sizing Design of stand- Alone Hybrid System Using a Fuzzy PSO," in *Artificial Intelligence and Heuristics for Smart Energy Efficiency in Smart Cities. IC-AIRES 2021. Lecture Notes in Networks and Systems, vol 361*, M. Hatti, Ed., Springer, Cham, 2022.

[35] D. Mazzeo, M. S. Herdem, N. Matera et al., "Artificial intelligence application for the performance prediction of a clean energy community," *Energy*, vol. 232, article 120999, 2021.

[36] Y. M. Al-Sharif, G. M. Sowilam, and T. A. Kawady, "Harmonic analysis of large grid-connected PV systems in distribution networks: a Saudi case study," *International Journal of Photoenergy*, vol. 2022, Article ID 8821192, 14 pages, 2022.

[37] N. D. Zamri and M. N. Abdullah, "A power system analysis for large scale solar photovoltaic system using PVSyst and ETAP," *Evolution in Electrical and Electronic Engineering*, vol. 3, no. 2, pp. 458–466, 2022.

[38] R. Smolenski, P. Szczesniak, W. Drozdz, and L. Kasperski, "Advanced metering infrastructure and energy storage for location and mitigation of power quality disturbances in the utility grid with high penetration of renewables," *Renewable and Sustainable Energy Reviews*, vol. 157, article 111988, 2022.

[39] M. Almaktar, A. Falah, Z. Hasan, A. Elbreki, and F. Mohamed, "Power quality assessment of Karabuk University's grid-connected microgrid under high penetration of PV generation," in *2022 International Symposium on Multidisciplinary Studies and Innovative Technologies (ISMSIT)*, pp. 472–477, Ankara, Turkey, 2022.

[40] J. Liu, X. Chen, S. Cao, and H. Yang, "Overview on hybrid solar photovoltaic-electrical energy storage technologies for power supply to buildings," *Energy Conversion and Management*, vol. 187, pp. 103–121, 2019.

[41] H. M. Ridha, C. Gomes, H. Hizam, M. Ahmadipour, A. A. Heidari, and H. Chen, "Multi-objective optimization and multi-criteria decision-making methods for optimal design of standalone photovoltaic system: a comprehensive review," *Renewable and Sustainable Energy Reviews*, vol. 135, article 110202, 2021.

[42] A. T. Azar and N. A. Kamal, *Design, Analysis and Applications of Renewable Energy Systems*, Academic Press, 2021.

[43] U. Das, S. Mandal, S. Bhattacharjee, and C. Nandi, "A review of different configuration of hybrid energy systems with case study analysis," *International Journal of Environment and Sustainable Development*, vol. 21, no. 1/2, pp. 116–137, 2022.

[44] S. Kumar, S. Sharma, Y. R. Sood, S. Upadhyay, and V. Kumar, "A review on different parametric aspects and sizing methodologies of hybrid renewable energy system," *Journal of The Institution of Engineers (India): Series B*, vol. 103, no. 4, pp. 1345–1354, 2022.

[45] S. Ishaq, I. Khan, S. Rahman, T. Hussain, A. Iqbal, and R. M. Elavarasan, "A review on recent developments in control and optimization of micro grids," *Energy Reports*, vol. 8, pp. 4085–4103, 2022.

[46] M. Sharafi, *Multi-objective optimal design of hybrid renewable energy systems using simulation-based optimization*, Elsevier, 2015.

[47] A. Kamjoo, *A decision support system for integrated design of hybrid renewable energy system, [Ph.D. thesis]*, Northumbria University, 2015.

[48] H. Asano, K. Yajima, and Y. Kaya, "Influence of photovoltaic power generation on required capacity for load frequency control," *IEEE Transactions on Energy Conversion*, vol. 11, no. 1, pp. 188–193, 1996.

[49] K. Ishaque, Z. Salam, and H. Taheri, "Modeling and simulation of photovoltaic (PV) system during partial shading based on a two-diode model," *Simulation Modelling Practice and Theory*, vol. 19, no. 7, pp. 1613–1626, 2011.

[50] E. Eimhjellen, *Optimal design of photovoltaic power plants, [M.S. thesis]*, The University of Bergen, 2018.

[51] A. Kaabeche, M. Belhamel, and R. Ibtiouen, "Sizing optimization of grid-independent hybrid photovoltaic/wind power generation system," *Energy*, vol. 36, no. 2, pp. 1214–1222, 2011.

[52] D. Rekioua, *Optimization of photovoltaic power systems modelization, simulation and control*, Green Energy and Technology, Springer London, 2012.

[53] R. Seyezhai, S. Karuppuchamy, and L. A. Kumar, *Recent Trends in Renewable Energy Sources and Power Conversion*, Springer, 2021.

[54] S. Tarak, B. Mounir, G. Adel, and M. Ahmed, "Matlab/Simulink based modelling of solar photovoltaic cell," *International Journal of Renewable Energy Research*, vol. 2, no. 2, 2012.

[55] M. P. Nguyen and M. P. Nguyen, "Mathematical modeling of photovoltaic cell/module/arrays with tags in Matlab/Simulink," *Environmental Systems Research*, vol. 4, no. 1, p. 24, 2015.

[56] A. Islam and I. Chowdhury, "Simulation of two diode model based PV solar cell/array: a simulink approach," in *1st International Conference on Research in Science, Engineering& Management (IOCRSEM 2014)*, New Delhi, India, 2014.

[57] A. Abubakar and R. N. Borkor, "Optimal extraction of photovoltaic cell parameters for the maximization of photovoltaic power output using a hybrid particle swarm grey wolf optimization algorithm," *Academic Journal of Research and Scientific Publishing*, vol. 3, no. 28, 2021.

[58] M. Maleki, "Estimation of hourly, daily and monthly global solar radiation on inclined surfaces: models re-visited," *Energies*, vol. 10, no. 1, p. 134, 2017.

[59] A. Abubakar, A. Musah, F. K. Owusu, and I. A. Addo, "Probabilistic method for estimating the level of reliability of solar photovoltaic systems for households in Ghana," *Asian Journal of Probability and Statistics*, vol. 15, pp. 38–53, 2021.

[60] E. W. Khatib and W. Elmenreich, *Modeling of Photovoltaic Systems Using Matlab: Simplified Green Codes*, John Wiley & Sons, 2016.

[61] A. Akšamović, S. Konjicija, S. Odžak, S. Pašalić, and S. Grebović, "DC cabling of large-scale photovoltaic power plants," *Applied Sciences*, vol. 12, no. 9, p. 4500, 2022.

[62] IEEE, *IEEE recommended practice for utility interface of photovoltaic (pv) systems*, IEEE Std, 2000.

[63] Sunpower, *Sun Power: An Introduction to the Applications of Solar Energy*, Elsevier, 2020.

[64] T. Parker, *How to maximize solar project value using inverter clipping*, Solar Power World, 2019.

[65] Polycab, *Polycab Solar Cables*, Elsevier, 2020.

[66] W. Dankoff, "How to choose an inverter for an independent energy system," *Home Power*, vol. 82, pp. 74–78, 2018.

[67] D. Dey and B. Subudhi, "Design, simulation and economic evaluation of 90 kW grid connected photovoltaic system," *Energy Reports*, vol. 6, pp. 1778–1787, 2020.

[68] Solar, *Calculating solar PV string size – a step-by-step guide*, Solar Energy Design, Wiley Online Library, 2014.

[69] W. Van Ackooij, R. Zorgati, R. Henrion, and A. Möller, "Chance constrained programming and its applications to energy management," in *Stochastic Optimization-Seeing the Optimal for the Uncertain*, IntechOpen Rijeka, 2018.

[70] J. Barrera, T. Homem-de Mello, E. Moreno, B. K. Pagnoncelli, and G. Canessa, "Chance-constrained problems and rare events: an importance sampling approach," *Mathematical Programming*, vol. 157, pp. 153–189, 2016.

[71] J. R. Birge and F. Louveaux, *Introduction to Stochastic Programming*, Springer Science & Business Media, 2011.

[72] F. B. Abdelaziz, "Solution approaches for the multiobjective stochastic programming," *European Journal of Operational Research*, vol. 216, no. 1, pp. 1–16, 2012.

[73] E. Bayraktar and S. Yao, "Optimal stopping with expectation constraint," 2020, http://arxiv.org/abs/2011.04886.

[74] Z. Zhou, C. Liu, and A. Botterud, "Stochastic methods applied to power system operations with renewable energy: a review," *International Journal of Environment and Sustainable Development*, vol. 32, 2016.

[75] A. Shapiro, D. Dentcheva, and A. Ruszczynski, *Lectures on Stochastic Programming: Modeling and Theory*, SIAM, 2021.

[76] K. Deb, *Multi-Objective Optimization Using Evolutionary Algorithms, Vol. 16*, John Wiley & Sons, 2001.

[77] F. Xu, J. Liu, S. Lin, Q. Dai, and C. Li, "A multi-objective optimization model of hybrid energy storage system for non-grid-connected wind power: a case study in China," *Energy*, vol. 163, pp. 585–603, 2018.

[78] X. Xia, J. Ji, C. S. Li, X. Xue, X. Wang, and C. Zhang, "Multiobjective optimal control for hydraulic turbine governing system based on an improved MOGWO algorithm," *Complexity*, vol. 2019, Article ID 3745924, 14 pages, 2019.

[79] S. Garcia and C. T. Trinh, "Comparison of multi-objective evolutionary algorithms to solve the modular cell design problem for novel biocatalysis," *Processes*, vol. 7, no. 6, p. 361, 2019.

[80] A. LaTorre, D. Molina, E. Osaba, J. Del Ser, and F. Herrera, "A prescription of methodological guidelines for comparing bio-inspired optimization algorithms," *Swarm and Evolutionary Computation*, vol. 67, article 100973, 2021.

[81] A. Sundaram, "Combined heat and power economic emission dispatch using hybrid NSGA II-MOPSO algorithm incorporating an effective constraint handling mechanism," *IEEE Access*, vol. 8, pp. 13748–13768, 2020.

[82] J. L. García, R. Monroy, V. A. Hernández, and C. A. Coello, "COARSE-EMOA: an indicator-based evolutionary algorithm for solving equality constrained multi-objective optimization problems," *Swarm and Evolutionary Computation*, vol. 67, article 100983, 2021.

[83] N. Riquelme, C. Von Lücken, and B. Baran, "Performance metrics in multi-objective optimization," in *2015 Latin American Computing Conference (CLEI)*, pp. 1–11, Arequipa, Peru, 2015.

[84] R. Pellegrini, A. Serani, G. Liuzzi, F. Rinaldi, S. Lucidi, and M. Diez, "Hybridization of multi-objective deterministic particle swarm with derivative-free local searches," *Mathematics*, vol. 8, no. 4, p. 546, 2020.

[85] S. Asumadu-Sarkodie and P. A. Owusu, "The potential and economic viability of solar photovoltaic power in Ghana," *Energy Sources, Part A: Recovery, Utilization, and Environmental Effects*, vol. 38, no. 5, pp. 709–716, 2020.

[86] V. Tiwaa, *Financing implications of going domestic solar photovoltaic energy: a case of selected homes in Brong Ahafo region, [Ph.D. thesis]*, Kwame Nkrumah University of Science and Technology, 2020.

[87] N. A. Obeng-Darko, "Why Ghana will not achieve its renewable energy target for electricity. Policy, legal and regulatory implications," *Policy, legal and regulatory implications, Energy Policy*, vol. 128, pp. 75–83, 2019.

[88] M. Taylor and E. Y. So, *Solar PV in Africa: costs and markets*, IRENA, Bonn, Germany, 2016.

[89] Joshua, "Ghana powers up: the largest solar plant in Africa is coming, Abuja," *Ventures Africa Magazine*, vol. 34, no. 11, pp. 2380–2390, 2016.

[90] K. Y. Kebede, "Viability study of grid-connected solar PV system in Ethiopia," *Sustainable Energy Technologies and Assessments*, vol. 10, pp. 63–70, 2015.

[91] S. Wang, X. Deng, H. Chen, Q. Shi, and D. Xu, "A bottom-up short-term residential load forecasting approach based on appliance characteristic analysis and multi-task learning," *Electric Power Systems Research*, vol. 196, article 107233, 2021.

[92] J. P. Marques de Sá, "Non-Parametric Tests of Hypotheses," in *Applied Statistics Using SPSS, STATISTICA, MATLAB and R*, J. P. Marques de Sá, Ed., Springer, Berlin, Heidelberg, 2008.

[93] M. M. Yazdi, "TOPSIS method for multiple-criteria decision making (MCDM)–package topsis," https://cran. http://r-project.org/web/packages/topsis.